THERAPEUTIC EFFECTS OF CONTROLLED-RELEASE MITOCHONDRIAL PROTONOPHORE TREATMENT AND ADIPONECTIN TREATMENT ON LIPID-INDUCED INSULIN RESISTANT MOUSE MODELS

Marshallplan-Jubiläumsstiftung
Austrian Marshall Plan Foundation
Fostering Transatlantic Excellence

Marshall Plan 2017/2018 Scholarship

FINAL REPORT

by

Michal PALLO

Clause of Confidentiality

SPERRVERMERK/CLAUSE OF CONFIDENTIALITY

Auf Wunsch der Firma/Institution/*upon request of* Name der Firma/Institution, ist die vorliegende BA/MA Arbeit für die Dauer von maximal 5 *Jahren* für die öffentliche Nutzung zu sperren/will the present BA/MA thesis be retained from public access for the period of max.5 years

Dauer der Sperre / period: **23 months**

Veröffentlichung, Vervielfältigung und Einsichtnahme sind ohne ausdrückliche Genehmigung der o.a. Firma und des Verfassers/ der Verfasserin bis zum genannten Datum nicht gestattet/*Unauthorized reading, publication and duplication will not be allowed without explicit consent given by the above-mentioned company and the author before:*

zu veröffentlichen am/*publication allowed*: **12/2019**

Unterschrift/*Signature*:

Name/Funktion. *Name/position*: **Gerald I. Shulman, MD, PhD/Principal Investigator**
Firma /Firmenstempel/Company/Seal:

VerfasserIn Abschlussarbeit/*Author thesis:* **Michal Pallo**

Unterschrift/*Signature*:

StudiengangsleiterIn /*Programme director:* **Prof.(FH) Mag. Dr. Harald Hundsberger**

Unterschrift/*Signature*:
Stempel FH/ *Seal*:

FH-SIC Medizinische & Pharmazeutische Biotechnologie
IMC
Piaristengasse 1
A-3500 Krems
StG-KZAHL 0571

Bestätigt am: /*Notified as of*: Klicken oder tippen Sie, um ein Datum einzugeben.

Acknowledgements

It is a great pleasure to thank all those who opened me the doors into the research universe and assisted me in composition of this report.

I owe my deepest gratitude to my supervisor and research advisor Dr. Gary W Cline, who made my research internship possible by affiliating me with his laboratory at Department of Internal Medicine at Yale University School of Medicine.

Also, my stay would have not been possible without the admirable work of our principal investigator Dr. Gerald I Shulman, who commissioned my project and has shown a great leadership and an exquisite guidance over the course of all the studies I participated in.

It is an honor to personally thank Kun Lyu, PhD student of Cellular and Molecular Physiology at Yale School of Medicine, who, as my personal tutor in all studies and a great friend, was always pleased to help me and revealed his sincere research enthusiasm which sparked my interest in science, positively influenced my scientific thinking and widened my life perspectives.

My gratitude further belongs to the PhD students, my colleagues and friends Xiruo Li and Yongliang Wang for their organizational work and planning done for each study.

All remaining laboratory members deserve a genuine word of thanks for their continuous support, additional guidance and willingness to readily answer all my questions as I explored the mechanisms and methods of treating diabetes.

I would further like to show my appreciation to the whole team at the IMC University of Applied Sciences in Krems, namely to my internal supervisor Dr. Christian Klein, my student advisor Dr. Barbara Entler and my program director Dr. Harald Hundsberger, for their prompt assistance and encouragement over the practical training semester.

Lastly, I am indebted to the Austrian Marshall Plan foundation for their valuable financial backing of my fellowship.

Abstract

Obesity-associated type 2 Diabetes Mellitus (T2DM) is one of the major risk factors for the cardiovascular disease, which is the leading cause of death globally. It is expected to affect up to 440 million people by 2045. One of the strongest risk factors for this condition is the spectrum of non-alcoholic fatty liver disease (NAFLD), which affects almost one third of the western population and manifests with hepatic and peripheral lipid-induced insulin resistance. Diagnosed only by a liver biopsy, the disease typically remains untreated, may lead to hepatocellular carcinoma, and existing therapies are largely ineffective.

The scope of this project was to advance laboratory's recent progress toward novel therapies targeting NAFLD-associated hepatic insulin resistance. Investigated were the effects of a blood glucose-regulating globular Adiponectin protein hormone and mitochondrial uncoupler 2,4-dinitrophenol on hepatic steatosis, insulin resistance and lipid metabolism in wild type and mutant lipodystrophic laboratory animal models in vivo, in an advanced stage of NAFLD by means of conventional analytic chemistry methods and mouse metabolic phenotyping approach.

The results of the studies have set a new direction for the development of NAFLD treatment. In contrast to the initial hypothesis, action mode of gAdiponectin in vivo came out to be more relevant to the muscle tissue, rather than to the white adipose tissue lipolysis in vivo. The efficacy of 2,4-dinitrophenol was negligible under our experimental conditions. Possible mechanisms for these results are currently being examined in a consecutive study phase.

A thorough elucidation of the insulin resistance pathogenesis would eventually deepen our understanding of not only uncontrollable related genetic disorders such as lipodystrophy, but also of the mechanisms of adipose tissue activity and its insulin resistance, to optimize our current therapeutic approach.

Table of Content

Clause of Confidentiality i

Acknowledgements ii

Abstract iii

Table of Content iv

List of Figures v

List of Abbreviations vi

1 Introduction 1

1.1 General 1

1.2 Lipid-induced insulin resistance 3

1.3 Role of adiponectin in reversing hepatic insulin resistance 6

1.4 Role of controlled-release mitochondrial protonophore (CRMP) in reversing hepatic insulin resistance 7

2 Aims 9

2.1 Experimental hypotheses 9

2.2 Experimental designs 10

2.2.1 gAdiponectin treatment 10

2.2.2 CRMP treatment 11

3 Materials and Methods 12

3.1 gAdiponectin treatment 12

3.1.1 Animal care 12

3.1.2 Body composition 12

3.1.3 Plasma non-esterified fatty acid assay 12

3.1.4 Liver and muscle TAG extraction and assay 13

3.1.5 Hyperinsulinemic-euglycemic clamp to assess insulin resistance 14

3.1.6 Hepatic and peripheral glucose metabolism by LSC 18

3.1.7 Lipid metabolism by GC-MS analysis of stable isotope tracer enrichment 22

3.1.8 Enzyme-linked immunosorbent assay of IL-6 and TNF-α 27

3.1.9 Statistical analyses 28

3.2 CRMP treatment 28

3.2.1 Animal care, genotyping by PCR and capillary electrophoresis 28

3.2.2 Body composition and metabolic cage study 30
3.2.3 Intraperitoneal glucose tolerance test (IPGTT) 30
3.2.4 Plasma insulin assay 31
3.2.5 Liver TAG extraction and assay 31
3.2.6 Plasma TAG assay 31
3.2.7 Plasma NEFA 31
3.2.8 Liver 2,4-DNP extraction 31
3.2.9 Statistical analysis 32

4 Results 33

4.1 gAdiponectin treatment 33

5 Discussion 36

5.1 gAdiponectin 36

5.2 CRMP treatment 37

6 Conclusion 38

References 40

List of Figures

Figure 1: Pathogenesis of insulin resistance in non-alcoholic fatty liver disease…….5
Figure 2: Schematic of the experimental hypothesis……9
Figure 3: Timeline and procedure of hyperinsulinemic-euglycemic clamp……..16
Figure 4: Liquid scintillation counting principle of β-particles……22
Figure 5: Schematic of GC-MS instrumentation……..24
Figure 6: Glycerol fragmentation by electron ionization……26
Figure 7: gAdiponectin results of the basal study……33
Figure 8: gAdiponectin results of hyperinsulinemic-euglycemic clamp study…….34
Figure 9: CRMP treatment results……35
Figure 10: Inflammation impairs ability of insulin to suppress lipolysis……..36

List of Abbreviations

T2DM…….type 2 diabetes mellitus

NAFLD……...non-alcoholic fatty liver disease

NASH…….non-alcoholic steatohepatitis

CRMP…….controlled-release mitochondrial protonophore

WHO……...world health organization

VLDL…….…..very low density lipoprotein

DNP……dinitrophenol

WAT…….…….……..white adipose tissue

CCL…….chemokine ligand

cAMP……..cyclic adenosine monophosphate

HGP……hepatic glucose production

FFA…….free fatty acids

HFD……high-fat diet

NEFA……..non-esterified fatty acids

FA-CoA……..fatty acyl-Coenzyme A

IRTK……insulin receptor tyrosine kinase

pIRS……insulin receptor substrate

FPLD……..familial partial lipodystrophy Dunnigan type

TAG……triacylglycerol/triglyceride

DAG……diacylglycerol

DNL……de novo lipogenesis

CM-R…….chylomicron remnants

FATP……..fatty acid transport protein

GLUT4……glucose transporter 4

PKC……....protein kinase C

HGP……hepatic glucose production

PC…….....…pyruvate carboxylase

PEPCK……..phoshoenolpyruvate carboxykinase

AMPK……AMP-activated protein kinase

FOXO1……..forkhead box protein O1

LpL…….lipoprotein lipase

ChREBP…….…..carbohydrate-responsive element-binding protein

FAS……fatty acid synthetase

TCA…….…..citric acid cycle

ACC……...acetyl CoA carboxylase

CPT-1…….....carnitine palmitotransferase 1

CLAMS……..comprehensive lab animal monitoring system

tSIE……..……..……transformed spectral index of the external standard

AEC……..… automated efficiency control.

U-^{13}C…….……universally labelled molecule with ^{13}C

MeOH……methanol

EtOH…….....ethanol

ACS…..…….acyl-CoA synthetase

MEHA……...3-methyl-N-ethyl-N(β-hydroxyethyl)-aniline

ACOD……acyl-CoA oxidase

ELISA……enzyme-linked immunosorbent assay

FBS……fetal bovine serum

PBS……phosphate binding buffer

v/v% ……..volume percent concentration

IPGTT……intraperitoneal glucose tolerance test

GC-MS……..gas chromatography-mass spectroscopy

LC-MS……...liquid chromatography-mass spectroscopy

GINF…….…….glucose infusion rate

CI……chemical ionization

EI……electron ionization

AUC…….……..area under the curve

IL-6……interleukin 6

TNF-α……tumour necrosis factor α

RT……..room temperature

SEM……..standard error of mean

PCR……..polymerase chain reaction

CE…….capillary electrophoresis

bp…….base pairs

cpm……..counts per minute

dpm……..disintegrations per minute

1 Introduction

1.1 General

In the recent years, we had the chance to observe a rapid industrialization as well as elevation of the Human Development Index (HDI) almost all over the world. Such a drastic change turned the human lifestyles, specifically in the countries with high HDI, more sedentary. Where food is in excess, obesity seems to expand at a critical rate and is now classified as epidemic by WHO [1].

With such a prevalence of obesity also grows the incidence of Type 2 Diabetes Mellitus (T2DM), which belongs to one of the successive diseases of obesity [2]. T2DM makes up 90% of diabetic patients worldwide [3] and novel scientific advancements do not allow us to ignore this issue.

T2DM includes a vast array of metabolic abnormalities observed simultaneously in multiple different tissues and sections of the organism. Out of all the complications of this disease, novel research focuses mostly at intervention into the progression of insulin resistance, either hepatic insulin resistance – failure of liver cells to respond to physiological insulin doses stemming from impaired molecular signaling in those cells, or peripheral insulin resistance – occurring in other tissues such as white adipose tissue, or muscle tissue. Such an absence of otherwise required molecular events leads to high fasting and postprandial plasma glucose levels, arising from increased rate of endogenous glucose production – gluconeogenesis, which explicitly characterized T2DM [4].

Abiding by a plethora of physiological principles, hepatic insulin resistance in type 2 diabetes is now thought to be caused by disruption of lipid homeostasis in the liver, defined as Non-alcoholic fatty liver disease (NAFLD), which is justified by its association with T2DM, as 90% of obese patients with T2DM also have NAFLD [5]. NAFLD now is the most common liver disorder in the Western world affecting a substantial 30% of the population of the United States, and rises in east and south Asian countries [6, 7].

NAFLD is a generic term for the spectrum that the disease comprises. The beginnings are defined by ectopic fat accumulation [8] – that means exceeding the internal lipid

disposal by mitochondrial β-oxidation system, or lipid export in VLDL particles by increased fatty acid flux from lipolysis and re-esterification of these fatty acids into triglycerides, and their subsequent deposition at tissues and organs other than those intended for lipid storage. This results in “fattening” of the organ in the long run. Usually, peripheral insulin resistance in skeletal muscle or white adipose tissue (WAT) occurs first and only later contributes to the development of hepatic insulin resistance [9]. Significantly elevated flux of free fatty acids seems to be the result of increase rate of triglyceride breakdown in WAT – lipolysis, or overabundant intake of dietary fats [4]. Liver steatosis can also arise from defective adipocyte maturation leading to localized or absolute redistribution of fat mass from storage sites into the ectopic sites, depending on the extent of the mutation that leads to such a syndrome. This phenomenon, however, is not plainly linked to obesity or dietary choices, but is rather a genetic condition which exacerbates the development of NAFLD. Correspondingly, this abnormal fat mass rearrangement critically increases the aggregation of plasma free fatty acids and thereby also elevates their flux into the liver or skeletal muscle tissue. These circumstances are thought to promote insulin resistance and diabetes in lipodystrophic patients [9-11].

Further progression in a more severe stage of the disease – non-alcoholic steatohepatitis (NASH), characterized by hepatic inflammation does not seem to be universal in all patients displaying hepatic steatosis. At that point, agglomerated fatty acids form free radicals [12] leading to peroxidation of lipids that cause collagen synthesis, exorbitant clustering of extracellular matrix proteins and eventual fibrosis by formation of Mallory’s hyaline in the cell and activation of stellate cells. All along, recruited are pro-inflammatory cytokines that grease the wheels of the inflammation [5, 13].

Current research advocates that such a stage transition might be affected by alterations in lipid metabolism by Tumor Necrosis Factor-α (TNF-α) and by glucose metabolism controlling and fatty acid breakdown regulating hormone adiponectin. Both having antagonistic effects in relation to each other [14].

If left unchecked, advanced liver fibrosis might drive the development of liver cirrhosis, which continuously displays insulin resistance, diminished insulin-mediated glucose disposal by up to 50% and significantly impaired glucose tolerance. Liver cirrhosis also

is perceived as a significant death factor in patients with diabetes and eventually leads to hepatocellular carcinoma, acute liver failure and death [5, 15].
While there is no established ordinance of these events, both NAFLD and NASH have a potential to lead to liver fibrosis, where the survival rate is the lowest. On top of that, NAFLD even displays certain non-modifiable risk factors such as body-mass index or race [16].

Nowadays there are novel pharmacologic interventions into the individual stages of NAFLD available. Specifically tested are anti-fibrotic agents such as inhibitor of lysyl oxidase-like 2 enzyme, which is the key matrix enzyme in collagen formation expressed in the liver. Further, orally available inflammatory chemokine CCL2/CCL5 inhibitors and liver cell death inhibitors, for instance anti-oxidants or inhibitors of apoptosis signal regulating kinases, since occurrence of fibrosis is the strongest predictor of mortality [17]. In the process of clinical trials are various other molecular inhibitors and agonists, however, it appears that the only means to reliably demonstrate the drug efficacy is to carry out liver biopsy. In addition, success rates of these trials indicate, that the attention should be given to the disease prevention in the first place, or alternatively target the most upstream point that triggers the disease development, instead of meddling with the consequences that may arise later downstream.

1.2 Lipid-induced insulin resistance

The action of hormone insulin, secreted by β-cells of pancreatic islets, is confined to an intracellular relay of molecular signaling, which allows for regulation of plasma glucose levels by triggering glycogen synthesis after glucose enters the cell, facilitated by GLUT2 transporter protein in the liver and GLUT4 transporters in the muscle tissue and WAT. Insulin receptor substrates (IRS) activated by bound insulin trigger Akt2 signaling cascade which in turn activates glycogen synthase to promote glycogenesis, and simultaneously, by nuclear exclusion of Forkhead box protein O1 (FOXO1) decreases transcription of gluconeogenic enzymes towards lowering hepatic glucose production (HGP). This is known as insulin-mediated plasma glucose disposal and is critical for maintenance of fasting and postprandial plasma glucose levels [4].

In white adipose tissue, insulin indirectly suppresses the rate of lipolysis by reducing cyclic adenosine monophosphate (cAMP) levels and thereby regulates plasma free fatty acid (FFA) levels, and in consequence, decreases HGP by reducing intramitochondrial hepatic acetyl-CoA which, as an allosteric regulator of gluconeogenic pyruvate carboxylase enzyme (PC), further curtails HGP. Enhancing HGP suppression in such wise may explain a rapid postprandial plasma glucose clearance. By suppression of lipolysis insulin lowers the influx of fatty acyl CoA (FA-CoA) that corresponds to the influx of FFA into a hepatocyte, facilitated by fatty acid transport proteins 2 and 5 (FATP2/5). This influx is later utilized for triglyceride (TAG) re-esterification. These events are crucial for maintaining blood glucose homeostasis as well as intrahepatic lipid balance [18-20].

In insulin resistant subjects, these mechanisms are disrupted (Figure 1.) Increased peripheral lipolysis of dietary fats by lipoprotein lipase (LpL), or, lipodystrophic ectopic fat redistribution significantly raise the flux of FFA into myocytes and cause intramyocellular fat accumulation and esterification FA-CoA substrate into diacylglycerols (DAGs) and TAGs, which impair the signaling cascade downstream of insulin receptor substrate 1 (pIRS1) by activation of Protein Kinase C isoform θ (PKCθ). Muscle glucose uptake is lessened, and excess glucose is diverted into the liver, where it serves as a substrate for *de novo* lipogenesis (DNL), contributing to hepatic lipid accumulation which characterizes NAFLD [18, 20]. This is a pre-diabetic state. Hepatic DNL from glucose naturally occurs as a response to postprandial hyperglycemia. Liver also takes up FFA from chylomicron remnants (CM-R) and plasma coming from WAT lipolysis to balance out increased plasma non-esterified fatty acid (NEFA) concentration. Raised flux of FFA into the hepatocyte triggers re-esterification of DAGs and TAGs, activating hepatic Protein Kinase isoform ε (PKCε) which impairs IRS signaling cascade in the like manner. Available FA-CoA heighten acetyl CoA levels by ongoing β-oxidation which, again, increases PC activity by allosteric regulation and thereby driving HGP by gluconeogenesis. Insulin-mediated glycogen synthesis is diminished in both, skeletal muscle and liver. Notably, glycerol coming from plasma TAG hydrolysis can also be converted to glucose by entering gluconeogenic pathway in the cell.

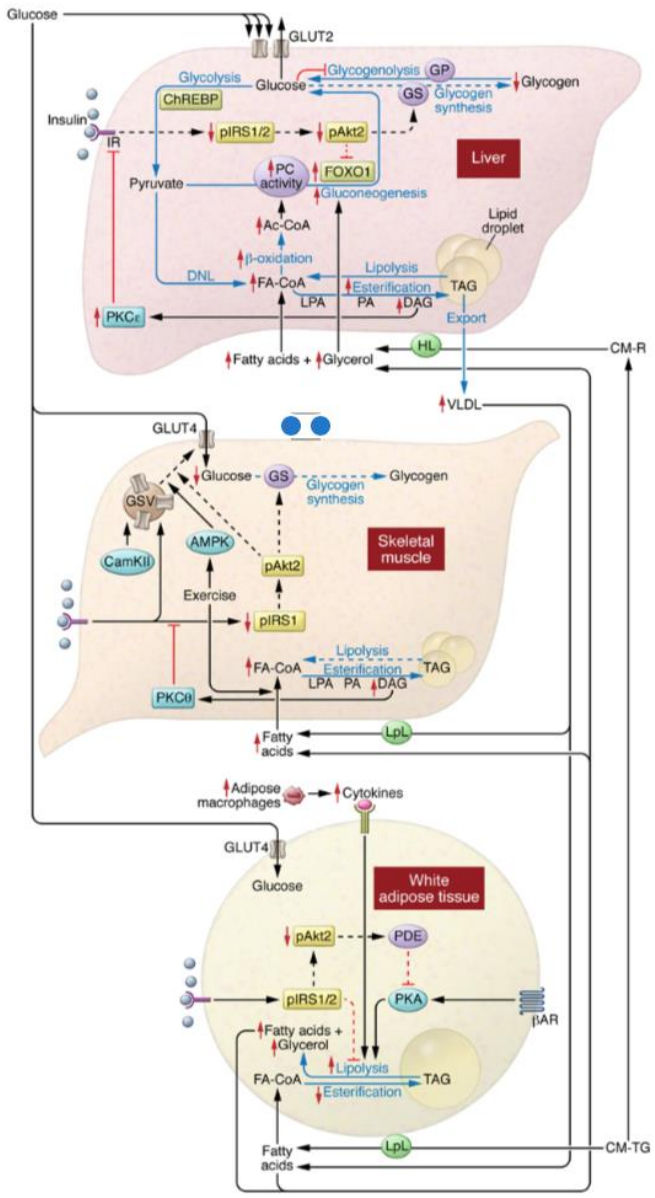

Figure 1.: Demonstration of the pathogenesis of insulin resistance in NAFLD. Peripheral insulin resistance in skeletal muscle and WAT typically precedes hepatic insulin resistance and later exacerbates hepatic steatosis according to these cellular mechanisms. Macrophage induced adipose lipolysis together with decreased skeletal muscle glucose uptake drive hepatic fat accumulation and result in hepatic insulin resistance [4].

T2DM patients additionally exhibit WAT inflammation due change of local microenvironment in adipose tissue that disrupts normal immune homeostasis. Release of pro-inflammatory cytokines and successive adipose macrophage infiltration promote WAT lipolysis of TAGs, also increasing the release of FFA and glycerol into the plasma. In this way macrophage-induced lipolysis raises and drives hepatic hyperlipidemia and promotes high fasting and postprandial glucose levels. Failure of insulin to suppress lipolysis accounts for suggested macrophage infiltration. Ultimately, hepatocytes become desensitized to insulin's leverage on maintaining intrinsic equilibria, resulting in characteristic complications of NAFLD and associated T2DM [4, 18-20].

With aim to study pharmacologic applications on the mechanisms of hepatic insulin resistance, Varman et al. [21] recognized a useful and reliable exhibition of NAFLD in rodent models by short-term high fat feeding, after which rodents displayed liver steatosis within the therapeutic range without peripheral fat accumulation. Mild degree of NAFLD seems to develop in the rodents within 3 day of high-fat feeding prior to peripheral insulin resistance, obeying the above-specified principles [22].

1.3 Role of adiponectin in reversing hepatic insulin resistance

In the process of pharmacologic elimination of hepatic steatosis as one of the initial complications of NAFLD spectrum, learning from body's endocrine system and taking the advantage of some of the secreted factors seems to be a viable option. Indicatively, adipocytes have an important function in regulating whole-body metabolism; they secrete a range of proteins – adipokines, most of which play their part in different inflammatory processes.

One of the most abundant adipose tissue-specific factors, adiponectin, also known as GBP-28, AdipoQ or Acrp30, is a novel protein hormone characteristic by its function to modulate blood glucose levels and fatty acid breakdown. Encoded by ADIPOQ gene and secreted into the bloodstream, its concentrations are higher in relation to other hormones, which makes it a scientifically attractive study subject [23]. Beneficial effects on reversal of hepatic steatosis, insulin resistance and associated NAFLD have been ascribed to adiponectin by numerous in vitro studies long ago. *Maeda et al*. suggested the function of adiponectin by evaluating plasma FFA and plasma TG clearance and observed increased TNF-α levels in epididymal WAT (eWAT) which might explain concurrent inflammation. Mouse myocytes exhibited diet-induced impaired insulin sensitivity together with reduced activity of insulin receptor substrate. Deficiency of adiponectin therefore contributes to insulin resistance and might therefore be considered as a risk factor for metabolic diseases, supported by evidence of obese patients shown to have lower adiponectin levels [24].

On top of that, *Fruebis et al.* investigated oxidative effects of protease-generated globular region of adiponectin (gAcrp30) treatment on mice and skeletal mouse myocytes and discovered that daily administration of globular adiponectin can reduce bodyweight without affecting food intake. In addition, acute treatment with gAdiponectin affects internal energy homeostasis by a rapid increase in mitochondrial FA oxidation [25]. These findings were later supported by *Iwabu et al.*, who described the mechanisms downstream of adiponectin receptor AdipoR1 signaling cascade. The findings suggest that increased FA oxidation in skeletal myocytes may be, in addition to already triggered oxidative metabolism by AMP-activated protein kinase (AMPK), also significantly enhanced by mitochondrial biogenesis [26].

In the light of these observations, *Qiao et al.* illustrated regulatory effects of adiponectin on lipid metabolism and recognized indirect adiponectin-stimulated inhibition of

lipolysis by suppression of Protein Kinase A mediated hormone sensitive lipase (PKA-HSL) in cultured mouse adipocytes, which is responsible for TAG hydrolysis and thereby decreases circulating FFA and thus also hepatic FFA flux [27].
To this end, *Holland et al.* showed that activation of adiponectin receptors AdipoR1 and AdipoR2 follows de-acylation of ceramides that normally interfere with previously outlined Akt signaling pathway. Ceramide catabolism then allows for heightened insulin action by active AMPK, leading to greater nutrient uptake, utilization, mitochondrial proliferation and cell survival [28]. In support of this, adiponectin even demonstrates enhanced suppression of hepatic HGP, first step towards alleviating diabetes [29].

It seems that there is ample evidence linking adiponectin to its effects to ameliorate insulin resistance in NAFLD. Because TNF-α and adiponectin have antagonistic effects on each other [14, 30] it could therefore be questioned, whether TNF-α really contributes to lowering adiponectin levels in obesity, aside from driving WAT inflammation that raises lipolysis. For this reason, restoring hypoadiponectinemia under such conditions may be an applicable strategy to benefit from anti-inflammatory effects of this adipokine in pursuit of protecting fatty liver from further inflammation, as well as attaining lost insulin sensitivity by decreasing FFA flux and disposing hepatic DAGs and TAGs. Boosted mitochondrial oxidation would restore necessary signaling cascades and improve insulin signaling, as indicated by referred studies.

1.4 Role of controlled-release mitochondrial protonophore (CRMP) in reversing hepatic insulin resistance

Increasing mitochondrial oxidation and by that lowering the rate of ectopic fat deposition in the liver was also shown to be effectively achieved by precise administration of liver-targeted controlled-release mitochondrial protonophore (CRMP). In detail, CRMP is a controlled-release formulation of the organic compound 2,4-dinitrophenol (DNP) which is a mitochondrial uncoupler of oxidative phosphorylation. In the cellular mitochondria, DNP acts as a proton shuttle across the mitochondrial membrane and thereby dissipates mitochondrial proton gradient, converting the energy obtained from substrate oxidation to heat [31]
Due to high toxicity and reported deaths from misuse of DNP, formulation with limited drug release was needed to be developed in order to safely deliver low doses of DNP

over a period of 12 to 24 hours, depending on diverse polymer coating combinations. The entire dosage is in this instance sized to deliver 1.0mg of DNP per kilogram of bodyweight in rodents. For this purpose, an extruded and drug layered DNP bead was found suitable for coating, and the final CRMP formulation was developed using hydroxypropylcellulose and ethyl cellulose drug coating system that substantially prolongs the absorption time after oral administration. Because DNP is by its nature subjected to first-pass metabolism effect in the liver [20], its disease-alleviating effects are expected to be observed in the liver the most. CRMP kinetics were confirmed by tissue DNP extraction to determine peak liver concentration. Effective therapeutic range was set between 1μM and 5μM [32].

By promoting profound increases in hepatic mitochondrial uncoupling, CRMP would cause increased citric acid cycle (TCA) flux in and therefore also increased hepatic FA oxidation that would clear accumulated DAGs and TAGs, restoring insulin signaling cascade and improving insulin sensitivity. In turn, plasma TAGs would be reduced as their import into the liver from plasma would be boosted and their export in VLDL particles into the plasma halted in order to maintain hepatic lipid homeostasis.

Insulin resistance alleviating effects of CRMP were indeed shown by *Perry et al.*; intragastric infusion of low dose of DNP significantly reduced plasma, liver and skeletal muscle TAGs by up to 80%, associated with a 60% increase in the TCA flux. Followed by an oral CRMP administration, similar effects were observed, together with decreased PKCε and θ isoforms translocation in liver and skeletal muscle respectively. Moreover, rats fed high-fat diet (HFD) were protected from the development of NAFD, since comparable effects were observed, in addition to decreased fasting plasma glucose and NEFA. CRMP also mitigated liver inflammation in Zucker Diabetic Fatty rats, as seen by liver enzyme normalization [32].

The efficacy of CRMP was further shown by *Abulizi et al.* on reversal of a lipodystrophic phenotype in AZIP/F-1 fatless mouse models of severe lipodystrophy. CRMP-treated group showed improved glucose tolerance and better insulin response during a hyperglycemic-euglycemic clamp study. Plasma glucose clearance was increased together with increased insulin-mediated HGP suppression, indicating a better insulin responsiveness overall. Insulin resistance and lipodystrophy are associated with hepatic steatosis and in this regard, concentrations of hepatic and plasma TAGs were almost halved along with hepatic DAGs in cytosol and membrane fractions and

therefore associated reductions in PKCε activity. Decrease in plasma TAGs may have also occurred due to their enhanced skeletal muscle disposal, where they could have been readily imported in response to the thermogenic potency of CRMP. Surprisingly, concentrations of several pro-inflammatory cytokines such as IL-2, IL-4 or IL-6 were also reduced, indicating reversal of liver inflammation [33].

Reductions in tissue ectopic fat depositions after CRMP administration were for the most part associated with improved whole-body insulin sensitivity [20] and therefore, these findings demonstrate potential efficacy of the CRMP as a therapeutic agent for NAFLD and NASH development to prevent liver cirrhosis and by such means induce a reversal of diabetes.

2 Aims

2.1 Experimental hypotheses

The aim of this thesis is to present my studies and the results I obtained, that are based on the findings of recent projects, by applying novel *in vivo* scientific and analytic methods to expand therapeutic possibilities for NAFLD associated T2DM treatment, for which there currently is a great unmet need.

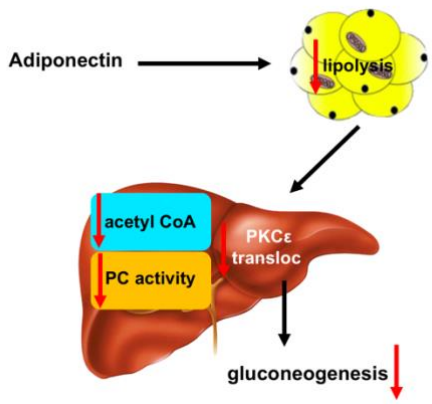

Figure 2: Schematic of the experimental hypothesis

In this regard, investigation of the beneficial effects of adiponectin *in vivo* in insulin resistant mice appears as a relevant and yet untested approach. Particularly, NAFLD was induced in standard C557BL/6J mice by 4-week *ad libitum* high-fat diet feeding, followed by gAdiponectin treatment. Its effects were assessed on the rates of lipolysis, degree of adipose tissue inflammation, insulin stimulated whole-body glucose utilization and extent of hepatic steatosis.

Hypothesis of the first study:

2-week subcutaneous administration of gAdiponectin will ameliorate insulin resistance and reverse hepatic steatosis by a substantial decrease in lipolysis in male mice. (Figure 2.)

The animals were studied at 12 weeks of age.

Aim of the second study was to advance laboratory's recent progress towards novel therapies targeting NAFLD-associated hepatic insulin resistance by mitochondrial uncouplers. The specific aim was to examine the effect of CRMP on glucose tolerance, hepatic steatosis and hepatic insulin resistance in LMNA mutant mouse model, mutation of which was shown to cause Dunnigan-type familial partial lipodystrophy (FPLD2) in humans. Hypothesis of the second study:
Oral CRMP administration in the length of 6 weeks will reverse hepatic steatosis, hypertriglyceridemia, improve insulin sensitivity and ameliorate type 2 diabetes in LMNA male mutant mice fed high-fat diet through increased hepatic oxidation.
The animals were studied at 8 weeks of age.

Lastly, it is noteworthy to mention, that for both studies, male mice of both strains were picked as the females are partially affected by hormonal and menstrual cycles, and protected against insulin resistance due to elevated estrogen levels, as turned out from years of experience.

2.2 Experimental designs

2.2.1 gAdiponectin treatment

To test our hypothesis *in vivo*, C557BL/6J laboratory male mice were divided into two groups of 8 – a gAdiponectin treated group and a control group for both, preliminary basal study – involving measurements of body composition by a vertical nuclear magnetic resonance system, fasting plasma glucose and plasma NEFA to obtain a rough indication of lipolysis, together with chloroform/methanol liver and muscle TAG extraction, and a clamp study, main component of which is a in vivo hyperinsulinemic-euglycemic clamp method.
In both studies, gAdiponectin was administered by a subcutaneous implantation of microosmotic pump 2 weeks prior to the experiments, which steadily released 0.25μg/hr of diluted gAdiponectin to attain a steady dose of 2.5 μg per mouse per day, continuously for 2 weeks. Hyperinsulinemic-euglycemic clamp was performed after a 4-week period, examining insulin sensitivity and insulin stimulated whole-body glucose disposal, by means of continuous intravenous [^{3}H]-glucose tracer infusion and a bolus injection of 2-deoxy-D-[1-^{14}C]-glucose. To determine relative lipolysis between these groups, co-infused were stable isotope [U-^{13}C]-potassium palmitate and [1,1,2,3,3-D5]-

glycerol, plasma enrichment of which was later spectroscopically detected by a gas chromatography-mass spectroscopy analysis (GC-MS), after sample derivatization. The results were reflected by a turnover rate, that represents rate of tracer appearance versus its clearance from plasma – uptake into the tissues. Liver and skeletal muscle were harvested and freeze-clamped in liquid nitrogen, and the tissues were subjected to TAG chloroform/methanol extraction to assess differences in hepatic steatosis between the groups. Cross-validation of results was resolved by plasma NEFA measurements. Lastly, to determine whether a change lipolysis was accompanied by a change in presence of pro-inflammatory cytokines, plasma and subcutaneous and epididymal white adipose tissue were subjected to an enzyme-linked immunosorbent assay of TNF-α and IL-6.

2.2.2 CRMP treatment

Transgenic lipodystrophic male mouse models FVB/N-Tg(Fabp4-LMNA*R482Q) were bred and 3 distinct groups of 12 formed – wild type FVB mouse group, mutant group and CRMP treated group, all groups high-fat fed. Treated group was given CRMP diet blend, containing additional 7.5g of DNP per kg of the diet, with mice absorbing an approximate dose of 50mg of DNP/day after *ad libitum* feeding. Transgenic mice expressed human mutant lamin A and C in adipocytes, which contain the most prevailing FPLD2 mutation R482Q, and as a lipodystrophic phenotype, were expected to be unable to accumulate fat, develop an enlarged and fatty liver and hence display decreased insulin sensitivity together with defects in thermogenesis [11]. Thermogenic effects of CRMP were thought to raise hepatic oxidation also in this form of severe lipodystrophy, even after a prolonged high-fat feeding of more than 10 weeks, resulting in a severe NAFLD.

Firstly, a Comprehensive Lab Animal Monitoring System (CLAMS) metabolic cage study was carried out to assess the parameters of drinking, feeding or calorimetry, followed by an intraperitoneal glucose tolerance test (IPGTT) to examine the effects of exogenous glucose delivery on systemic glucose clearance which ultimately correlates with *in vivo* insulin sensitivity. To investigate the extent of NAFLD reversal, animal livers were harvested and freeze-clamped to carry out TAG extraction. Effects of CRMP on reversal of hypertriglyceridemia were evaluated by a plasma TAG assay from inferior vena cava in fasted state. To associate the outcomes of the treatment

with an estimate of required hepatic DNP concentration, livers were subjected to organic DNP extraction and successive analysis by a liquid chromatography-mass spectroscopy (LC-MS) system.

3 Materials and Methods

3.1 gAdiponectin treatment

3.1.1 Animal care

All mice were bred, kept and fed at the Yale Animal Resource Centre (YARC), which provided a reliable animal housing facility. Mice had an *an libitum* access to food and water, supply of which was regularly monitored. Room temperature was maintained in the range from 21.5°C to 22°C together with an automatic 12h day/night light cycle switching. A maximum of 4 littermates were kept in one cage and prior to the hyperinsulinemic-euglycemic clamp were separated. Animals were fed a 60% kcal% fat diet, source of fat being lard and soybean oil, source of carbohydrates a mixture of maltodextrin and sucrose, and L-cysteine and 30 mesh casein as a protein supply. This diet additionally contained vitamin blends and essential micronutrients to guarantee otherwise a balanced nutritional content. Animals were ordered from the Jackson Laboratory and high-fat diet D12492 regularly supplied from Research Diets.

3.1.2 Body composition

To evaluate the effects of gAdiponectin on total bodyweight, fat mass and lean body mass, a vertical ^{1}H-nuclear magnetic resonance (NMR) spectroscopy system Minispec MQ Series (Bruker) was used, which reliably prevents the movement of the animal. The system looks at NMR sensitive nuclei such as Hydrogen or Fluorine, using permanent magnetic field and radiofrequency energy. This measurement was conducted prior to a hyperinsulinemic-euglycemic clamp after a 2-day recovery, to eliminate transport stress to the greatest extent. Adopted from https://mmpc.org.

3.1.3 Plasma non-esterified fatty acid assay

Levels of plasma NEFA (plasma FFA) have been suggested long ago to be elevated in obese subjects, and therefore can be associated with fatty liver disease and serve as a rough indication of expanded WAT lipolysis [34]. This imbalance in fatty acid

metabolism is a significant factor in development of insulin resistance by ectopic fat accumulation. Excess plasma NEFA are usually transported to muscle and liver, where they re-esterify. In this regard, it is considered a supplementary index of insulin resistance. To evaluate the effects of gAdiponectin treatment on WAT lipolysis, an in vitro enzymatic-colorimetric method assay for quantitative determination of NEFA in serum was conducted in the preliminary basal study. NEFA assay quantifies the whole-body concentration of NEFA appearing in plasma after TAG hydrolysis.

HR Series NEFA assay (Wako) relies upon acylation of coenzyme A by fatty acids in the presence of added acyl-CoA synthetase (ACS). Acyl-CoA produced is oxidized by added acyl-CoA oxidase (ACOD) with generation of hydrogen peroxide. In the presence of hydrogen peroxidase, an oxidative condensation of 3-methyl-N-ethyl-N(β-hydroxyethyl)-aniline (MEHA) with 4-aminoantipyrine is permitted, which forms a purple colored product which is colorimetrically measured at 550 nm.

Blood plasma was obtained directly from mouse inferior vena cava under anesthesia with isoflurane gas.

1. A standard curve of absorbance vs. concentration was created by adding increasing volume of oleic acid at 1 mEq to glass tubes.
2. 10 μL of plasma is added into new glas tubes.
3. 225 μL of color reagent A is added, which contains ACS, Coenzyme A and 4-aminoantipyrine
4. 75 μL of color reagent B is added, which contains ACOD and peroxidase in MEHA.
5. Samples are vortexed and let sit at RT for 10 min to react completely. With increasing concentration of NEFA was increasing the intensity of the color.
6. The absorbance was read at 560 nm (signal) and 670 nm (background). Signal absorbance was subtracted from the background absorbance and NEFA concentration was calculated with linear interpolation of the standard curve. Values are represented in mEq/L.

3.1.4 Liver and muscle TAG extraction and assay

After animal euthanasia, liver and gastrocnemius muscle were dissected out and freeze clamped. These tissues were subjected to organic extraction and quantification of TAGs by colorimetric Triglyceride-SL assay reagent (Sekisui), to examine the effects of the treatment on the hepatic steatosis. Triglycerides are hydrolyzed to FFA and

glycerol and in the presence of ATP and glycerol kinase, glycerol is phosphorylated to yield hydrogen peroxide. The hydrogen peroxide causes oxidative coupling of p-chlorophenol and 4-aminoantipyrine, producing a red quinonemine dye complex. Fluid lipids were separated and extracted from other constituents with $CHCl_3$/MeOH (J.T. Baker) (2:1, v/v%). Absorbance at 520nm due to formation of the dye complex is directly proportional to the concentration of triglycerides in the sample.

1. 50 - 100 mg of frozen tissues was weighted into polypropylene tubes.
2. 1 mL of precooled 2:1 $CHCl_3$/MeOH was added and tissues were homogenized with metal beads in Tissue Lyser (Qiagen) at 30 Hz (oscillations/minute).
3. Homogenized sample was transferred to a scintillation vial and washed with another 1 mL of precooled 2:1 v/v% $CHCl_3$/MeOH.
4. Samples were shaken for 4 hours and treated with 1M H_2SO_4 to precipitate proteins. A middle layer between the lower organic, lipid containing layer and the upper aqueous layer was formed.
5. 10 μL aliquot of the organic layer was dried down under N_2 gas.
6. Dried lipids were re-suspended in 1 mL of TAG reagent and absorbance was read at 520nm. The concentration of TAGs was calculated from a wide standard curve using DC-Cal Multi-Analyte calibrator (Sekisui). Results were expressed in mg/g of the tissue.

3.1.5 Hyperinsulinemic-euglycemic clamp to assess insulin resistance

Hyperinsulinemic-euglycemic clamp is considered the “gold-standard” method for evaluation of insulin action in vivo. It is applied to various species including humans, rats, dogs or mice. Clamps are regularly employed in research setting to study conscious transgenic animal models of obesity and diabetes, since insulin sensitivity is clinically assessed to predict the risk and extent of type 2 diabetes in. A miniaturized clamp for animal models appears to resolve the limitations of other insulin resistance assessment methods, as it estimates HGP under insulin stimulated conditions and its suppression by the insulin. Hyperinsulinemic state is achieved by primed and later continuous insulin infusion at a constant rate which rapidly raises systemic insulin levels. Hypoglycemia is countered by an intravenous infusion of glucose at a variable rate (GINF) to achieve a “euglycemic” steady state in the last 30 min of the experiment. Here, variable GINF directly correlates with the whole-body insulin sensitivity. Higher

GINF at the steady states indicates an insulin sensitive subject - glucose is sharply utilized and taken up by the tissues and therefore more glucose is required to maintain euglycemia. In contrast, insulin resistant subjects exhibit a significantly lower GINF as the glucose utilization and clearance from plasma is impaired, as Figure 1. demonstrates. GINF is adjusted according to plasma glucose levels, which are sampled in brief intervals over the whole experiment. Incorporation of [3-^{3}H]-glucose into the glucose infusate allows for calculation of whole body glucose turnover, which is the rate of plasma glucose appearance (HGP + glucose infusion) in versus the rate plasma glucose disappearance (uptake), together with insulin's ability to suppress HGP, leading to overview of whole-body and hepatic insulin sensitivity. Injection of a 2-deoxy-D-[1-^{14}C]-glucose bolus, a non-metabolizable glucose analogue, right after achieving euglycemia allows for assessment of skeletal muscle glucose uptake, to specifically determine insulin sensitivity on the periphery. Experiment consists of a basal - non-insulin stimulated - phase at the beginning, and an insulin-stimulated clamped phase [35, 36].

1. All infusions are administered via catheterized jugular vein. 6 days prior to the clamp, animals underwent a surgical catheterization. After ketamine/xylazine anesthesia, a PE10 silastic catheter (Helix Medical) was surgically inserted into the jugular vein and immediately heparinized to prevent thrombosis within the tubing.
2. An average of 3 mice could be clamped per day. After an overnight fast (~12h) done to reduce the effect of gastrointestinal absorption, animals were placed into oversized restrainers and 0.5cm tips of their tails were cut and tails taped and tethered to the restrainer end. Blood was sampled from tail capillaries.
3. Infusion of [3-^{3}H]-glucose (Perkin Elmer, 5mCi in 5 ml EtOH) at basal state was initiated using a microdialysis pump (CMA 402 Syringe Pump) at 0.05 μL/min/mouse. Denoted as t = -120 min in the Figure 2. This was done to assess the basal rate of whole body glucose turnover.
4. 80 μL of blood was collected at the end to measure plasma glucose and [^{3}H]-glucose tracer concentrations. These are the basal clamp parameters.

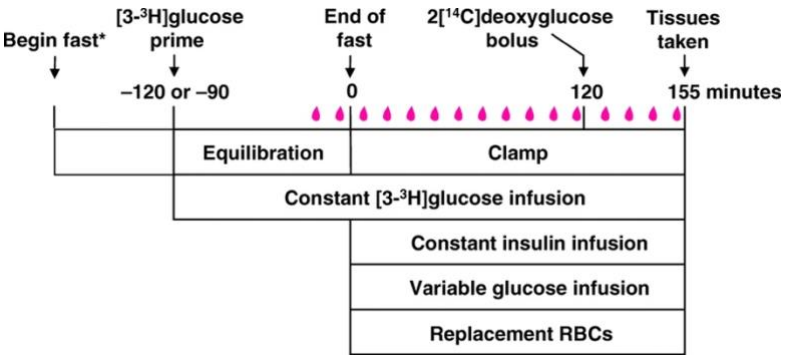

Figure 3: Timeline and procedure of hyperinsulinemic-euglycemic [35]

5. Systemic insulin levels were raised at t = 0 min. 150 mU/kg body weight of regular human insulin (Novolin, Novo Nordisk) were infused over 3 minutes. Priming is necessary to achieve steady state faster.

6. Glucose tracer was dissolved in the insulin infusate syringe, and was constantly infused until t = 155 min at 0.1 μCi/min/mouse with insulin infused at 2,5 mU/kgBW/min.

7. To assess lipid metabolism, stable isotope FA tracer [U-^{13}C]-potassium palmitate and [1,1,2,3,3-^{2}H]-glycerol (Cambridge Isotopes Laboratories, Inc.) tracers were additionally dissolved in the insulin infusate, and simultaneously infused at 300 μg/kg/min (potassium palmitate) and 75 μg/kg/min (glycerol). Tracer enrichment was analyzed by GC-MS and whole body lipolysis was calculated, both to be described in section 3.1.5.

8. 20% dextrose for intravenous use (Hospira, Inc., ph 4.3) was infused at variable rate, ranging from ~1.3 μL/min up to ~3 μL/min for insulin resistant subjects, and ~2.0 μL/min up to ~8 μL/min for insulin sensitive subjects. The rate is largely also bodyweight dependent, which is why it's necessary to carry out clamps in animals with comparable bodyweights.

9. 20 μL of blood was collected from tail tips in 10-15 min intervals into hematocrit tubes coated with ammonium heparin (Drummond, Mylar Wrapped x75mm) with a stagger time of 8 minutes between each mouse. Plasma glucose was recorded in mg/dL for each time point using YSI Biochemistry Analyzer 2700 Select, which provided analysis within a minute of time without additional plasma preparation.

10. To evaluate muscle-specific glucose uptake, a 10 μCi bolus of 2-deoxy-D-[1-^{14}C]-glucose (Perkin Elmer, 1 mCi in 10mL EtOH) was administered t = 85 min, time-point

at which we assume most of the animals reached euglycemia, indicated by plasma glucose levels in the range of ~100 mg/dL up to 130 mg/dL.

11. 40 μL of blood collected at t = 90, 100, 110, 120, 130 and 140 min. This plasma was used to carry out a biochemical tracer assay of [3-^{3}H]-glucose by plasma deproteinization.

12. Animals were anesthetized by infusion of 150mg/kg of Pentobarbital Sodium (Fatal Plus) and liver, gastrocnemius muscle from hind limbs and eWAT tissue were harvested and rapidly freeze-clamped in liquid N_2. All samples were stored for later biochemical analysis at -80°C.

All infusion values are based on standard protocol shown to be effective in delivering comparable results within physiological conditions [35]. Radioactive isotope tracers had to be dried down in the Fisher Scientific Isotemp® Vacuum Oven one day before, in their respective amounts needed to achieve desired infusion rate. These amounts depended on the number of mice that survived the surgery and their bodyweight, and were planned for clamp that day. Usually, 900μL of stock 20% dextrose was used per mouse, and 90μL of stock [3-^{3}H]-glucose reconstituted in 7mL of saline and 700μL of stock 2-deoxy-D-[1-^{14}C]-glucose were dried. This step was necessary to dispose EtOH solvent, that would otherwise distort the consciousness of the animal. Stable isotope tracers together with insulin had to be dissolved in artificial plasma, that contained BSA. BSA prevents insulin adhesion to the glass tube, in which it was prepared, and solubilizes potassium palmitate in saline by formation of BSA-palmitic acid complex.

Key aspect of performing mouse clamps is the proficiency of GINF adjustment, which develops with experience. This is crucial, as there is limited time to achieve the steady state. We assume each next GINF adjustment based on the previous plasma glucose concentrations changes. Data are usually inherently noisy due to a very high metabolic rate. In some variants of this method, erythrocytes may be transfused to replenish blood content, or [^{3}H]-glucose may be primed, as indicated by Figure 2.

3.1.6 Hepatic and peripheral glucose metabolism by LSC

To evaluate effects of gAdiponectin on hepatic and peripheral glucose metabolism under insulin-stimulated and non-stimulated conditions, radiolabeled glucose tracers are commonly employed for research. Choice of the tracers is based on their detection method, traced substrate and price, and they must follow same metabolic fate as the traced substrate - tracee. Radioactive isotope tracers are usually almost identical to tracees, differing only in one or more atoms which are isotopically labelled. Isotopes of [3-^{3}H]-glucose and 2-deoxy-D-[1-^{14}C]-glucose both disintegrate by β-particles emission, and their presence can be detected by liquid scintillation counting (LSC). A remarkably long half-life of tritium and [^{14}C] ensures an accurate measurement even after a long time. In addition, traced glucose shows a very low abundance of these radioisotopes, leading to negligible signal/background noise ratio. By comparison, stable isotope atoms in tracers do not spontaneously disintegrate, and their identification is analyzed by GC-MS [37]

[3-^{3}H]-glucose

Using [^{3}H] glucose was especially a reasonable choice in metabolic research, as Hydrogen is highly abundant in organic compounds, despite its low detection sensitivity. In this regard, hepatic glucose metabolism is represented by HGP and whole body glucose metabolism by whole-body glucose turnover. These two indicators were relatively compared within the groups, at basal and clamped state, HGP and its suppression showing insulin's action on gluconeogenesis, and whole body glucose turnover. Both were calculated at the basal as well as clamped state.

<u>The basal glucose turnover</u> (Rd) calculated at the end of basal infusion period as:

$$Rd = \frac{basal\ [3\mathrm{H}]glucose\ infusion\ rate}{specific\ activity\ of glucose}[mg\ (kg.min^{-1})]$$

Because HGP is the only source of glucose introduced into the system at the basal state, the basal glucose turnover also represents the <u>basal rate of HGP</u>. Specific glucose activity (SA) is the tracer enrichment in the plasma, which is ratio of labelled glucose versus total glucose amount. SA is due to radioactive nature of tracer expressed in dpm/μmol, where dpm reflects number of atoms decayed at the source

in one minute - disintegrations per minute. This is automatically calculated by liquid scintillation counter based on this relationship:

$$dpm = \frac{cpm - background\ cpm}{\%\ counting\ efficiency}$$

where cpm is count per minute - number of atoms measured as decayed and were detected by the source. 20μL of plasma at t = 0 min were used for this measurement. Under insulin stimulated conditions, source of glucose is HGP together with exogenous glucose infusion (20% dextrose). At steady state, their appearance equilibrates with peripheral glucose disappearance, allowing us to calculate "clamp" whole-body glucose turnover:

$$Rd = \frac{clamp\ [3H] glucose\ infusion\ rate}{specific\ activity\ of\ glucose\ during\ final\ 50\ \mathrm{min}} [mg\ (kg.min^{-1})]$$

To calculate "clamp" HGP:

$$clamp\ HGP [mg\ (kg.min^{-1})]\ = Rd - glucose\ infusion\ rate$$

20μL of plasma at t = 140 min were used for this measurement.
During clamp, insulin maintains glucose homeostasis by suppression of HGP and increasing glucose utilization in peripheral organs. Hence, HGP is expected to be lower and glucose turnover to be higher.

2-deoxy-D-[1-^{14}C]-glucose

It appears that muscle tissue is the principal site of glucose utilization in vivo and hence lower proportion of glucose is shuttled into other peripheral tissues [38]. To this end, 2-DG traces skeletal muscle tissue-specific glucose accumulation under insulin stimulated condition. Result would reflect partial peripheral glucose metabolism. Bolus injection of as little as 10 μCi of 2-[1-^{14}C]-DG was shown to accurately assess muscle glucose uptake. Absence of oxygen on this ^{14}C-labelled molecule causes trapping of the molecule within the cell after phosphorylation into 2-[1-^{14}C]-DG-phosphate by hexokinase. After injection, insulin shuttled 2-[1-^{14}C]-DG together with glucose into myocytes through GLUT4 transporter protein. Tissue 2-[1-^{14}C]-DG-phosphate

concentrations were determined by its separation from remaining 2-[1-^{14}C]-DG by anion-exchange column and LSC.

The glucose uptake rate (Rg) was calculated from plasma 2-[1-^{14}C]-DG decay profile expressed on an exponential curve fitting intracellular 2-[1-^{14}C]-DG-phosphate content:

$$Rg = \frac{Cp\ Cm}{\int_{t=0}^{45} Cp(t)dt} = [glucose]\frac{muscle\ levels\ of\ [14C\ 2DG-6-P]}{\int_{t=0}^{45}[14C-2DG](t)dt}[mg\ (kg.min^{-1})]$$

where C_p reflects plasma glucose concentration at steady state, C_m is tissue 2-[1-^{14}C]-DG-phosphate concentrations and $C_p(t)$ expresses plasma 2-[1-^{14}C]-DG concentration *t* minutes after the bolus. C_p and $C_p(t)$ were measured by plasma deproteinization tracer assay, C_m by tissue tracer extraction, both of which followed LSC.

Plasma deproteinization tracer assay

Following clamp, plasma [3-^{3}H]-glucose and 2-deoxy-D-[1-^{14}C]-glucose concentrations were determined in 10 mL plasma at t = 0, 90, 100, 110, 120, 130, 140 min. by deproteinization and LSC. Two sample sets, non-dry (suspension by 175 μL of ddH_2O) and dry (no ddH_2O) were prepared. If needed, non-dry set would be used to calculate glycolysis from the rate of increase in plasma $^{3}H_2O$ concentrations. This method was not employed.

1. Plasma samples were thawed and centrifuged down.
2. 25 μL of $ZnSO_4$ and 25 μL $Ba(OH)_2$ were introduced to precipitate unwanted plasma proteins. Samples were centrifuged at 12000 rpm (Eppendorf)
3. 2 sets of scintillation vials were prepared. 175 μL ddH_2O were added into non-dry set.
4. 25 μL of supernatant was added to non-dry set of vials, as well as 3 mL of scintillation cocktail (Ultima Gold, Perkin Elmer). Dry set of vials was dried in vacuum oven overnight completely, and scintillation cocktail was added the next day.
5. Samples were vortexed and radioactivity was measured by LSC (Tri-Carb 3100TR, Perkin Elmer).

Muscle tissue 2-[1-^{14}C]-DG-phosphate extraction

To run LSC of 2-[1-^{14}C]-DG-phosphate, the compound had to be extracted from dissected gastrocnemius muscle and separated from 2-[1-^{14}C]-DG by anion-exchange chromatography.

1. Prepared were: frozen muscle tissues, liquid N_2, dry ice, scintillation vials, labelled glass tubes and set of anion-exchange columns (Polyprep Bio-Rad AG 1-X8 resin, 100-200 mesh in ionic Cl^- form), water bath at 100°C, ddH_2O and 0.2M Formic Acid (J.T. Baker, 88%)/0.5M Ammonium Acetate (Sigma) at pH 4.9.
2. 70 - 100 mg of muscle tissue was weighted into glass tubes and 10X volume of ddH_2O was added (e.g. 1000 μL for 100 mg).
3. Muscle tissue was homogenized.
4. Homogenized samples were foil-wrapped and put into water bath for 10 min.
5. Samples were sealed with Parafilm and centrifuged at 4000 rpm (Eppendorf). Anion-exchange columns were washed 3x with 2.5 mL ddH_2O in the meantime.
6. 40 μL of supernatant was added to scintillation vials and filled up to 500 μL with ddddH_2O. 3 mL of Ultima Gold scintillation cocktail was added, samples were vortexed and ^{14}C counted. This set represented total ^{14}C concentration.
7. 400 μL of supernatant was transferred to the columns. Columns were washed 3x with ddH_2O. At this step, P^- group has higher affinity for the resin than Cl^- and competitively binds. Washing the columns elutes unbound 2-[1-^{14}C]-DG, which was collected and counted by LSC.
8. Bound 2-[1-^{14}C]-DG-phosphate was eluted by 3x washing with 2 mL 0.2M Formic Acid/0.5M Ammonium Acetate which changes the pH environment and disrupts P^- binding. Eluate was collected, cocktail added and ^{14}C concentration counted.

Radiometric detection of ^{3}H and ^{14}C by liquid scintillation counting

Liquid scintillation counting was generally used for quantification of radioactive alpha or β-particle emission in liquid our samples. Radiolabeled analytes get uniformly distributed in the solvent is of 2,6-diisopropylnaphtalene-based scintillation cocktail upon dissolving. β-particles emitted from ^{3}H and ^{14}C decay ionize the solvent, π-cloud

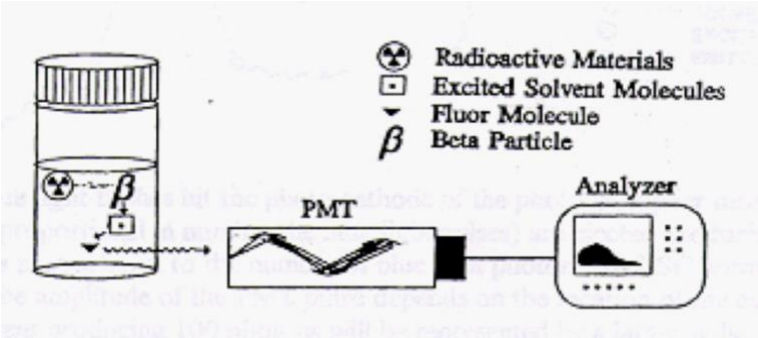

Figure 4: Liquid scintillation counting principle of β-particles [38].

of the aromatic ring absorbs this energy. Absorbed energy is transferred back and for the between solvent molecules until they reach the primary scintillator Depending on the absorbed energy, the primary scintillator emits flashes of blue light that is detected by photomultiplier tube (Figure 3.). The "scintillation" corresponds to the total number of flashes together with light intensity both of which are proportional to the initial energy emitted from the β-decay [39].

To account for a generally low ^{3}H counting efficiency, Ultima Gold cocktail of our choice directly addresses the problem of a generally low ^{3}H counting efficiency, as it's primarily suited for ^{3}H detection. The amount of cocktail used (3 mL) corresponds to the maximum countable capacity of radioactivity, that also is in our sample.

Tri-Carb 3100TR operates in various pre-set running protocol. Our protocol was optimized to simultaneously count ^{3}H and ^{14}C through designated radionuclide channels. Counting time was 10 minutes/sample, with background signal subtraction from 1st blank sample, without luminescence correction mode, in cpm and dpm units. Efficiency of the counting was expressed as a function of the quench indicator "*tSIE/AEC"* which serves as a calibration factor for imposed quenching from impurities, such as colored or chlorine-like compounds [40]. Analysis was performed on QuantaSmart software.

3.1.7 Lipid metabolism by GC-MS analysis of stable isotope tracer enrichment

The use of stable isotopes is commonly employed to assess lipid metabolism, particularly to study fatty acid flux in vivo by calculating fatty acid turnover rate. From this perspective, turnover will portray lipolysis from peripheral WAT, which is the major source of fatty acid appearance in plasma at the steady state during clamp. In contrast to radioactive tracers, stable isotopes are safer to use, measured at a very high precision, but amounts infused must be large enough to be detected by GC-MS, where they are separated based on their mass to charge ratio at the detector. For an effective detection, we aim to enrich the blood plasma by 1-2%. Stable isotope enrichment is

express as atom per excess (APE) and accounts for the presence of natural abundance of isotopes in the plasma [37, 41]:

$$APE = \frac{tracer}{tracer + tracee} \times \frac{100}{1}$$

higher than 1-2% may affect adversely the metabolism. Since adipocytes hydrolyze TAGs to FA and glycerol, [U-^{13}C]-potassium palmitate (98%+) and [1,1,2,3,3-^{2}H]-glycerol (99%) (Cambridge Isotopes Laboratories, Inc.) tracers were chosen - palmitic acid is the most representative of all fatty acids in plasma, glycerol was traced to cross-validate the results [42]. At the steady state, rate of appearance equilibrates with the rate of disappearance, which corresponds to the rate of WAT lipolysis under insulin stimulated conditions (for distinction labelled as Ra):

$$Ra = \frac{tracer\ infusion\ rate}{APE}\ [\mu mol(kg.min^{-1})]$$

Prior to clamp, 400 μL of palmitate tracer out of 20 mg/mL stock and 15.4 μL of glycerol tracer out of 630 mg/mL stock were combined with 3600 μL of artificial plasma, dissolved in saline and insulin as section 3.1.7 outlined. To assess the rate of lipolysis, the plasma tracer APE was analyzed on GC-MS.

GC-MS analysis of [U-^{13}C]-potassium palmitate and [1,1,2,3,3-^{2}H]-glycerol of APE

GC-MS is a well-established and sensitive technique used in many laboratories to distinguish different isotopes in a wide range of components, even when the enrichment is extremely low. The sample was vaporized and injected into the chromatographic column, following elution of separated neutral constituents according to their retention times. These were ionized within the ion source (Figure 4.) which is either electron ionization (EI) or chemical ionization (CI). EI employs an electric light bulb filament to bombard the molecules with electrons at 70eV of energy and upon the collision, a molecular cation M^{+} forms, which if retains enough energy, is fragmented into neutral fragments based on a specific fragmentation pattern, which depends on the strength of molecular bonds. This may lead to loss of isotopically labelled atom, so the pattern must be understood to determine the enrichment. CI is a milder ionization technique, also using the light bulb filament, but ionization is buffered by isobutane gas and results in little or no fragmentation. Ions then pass through quadrupole mass analyzer which separates them according to their mass to charge ratio - *m/z*. Separated ions hit the electron multiplier tube - the detector, which produces mass spectrum, showing us the distribution of all ions in our sample by mass [43]. Plasma samples had to be volatilized by chemical derivatization, making them easily vaporizable for column injection.

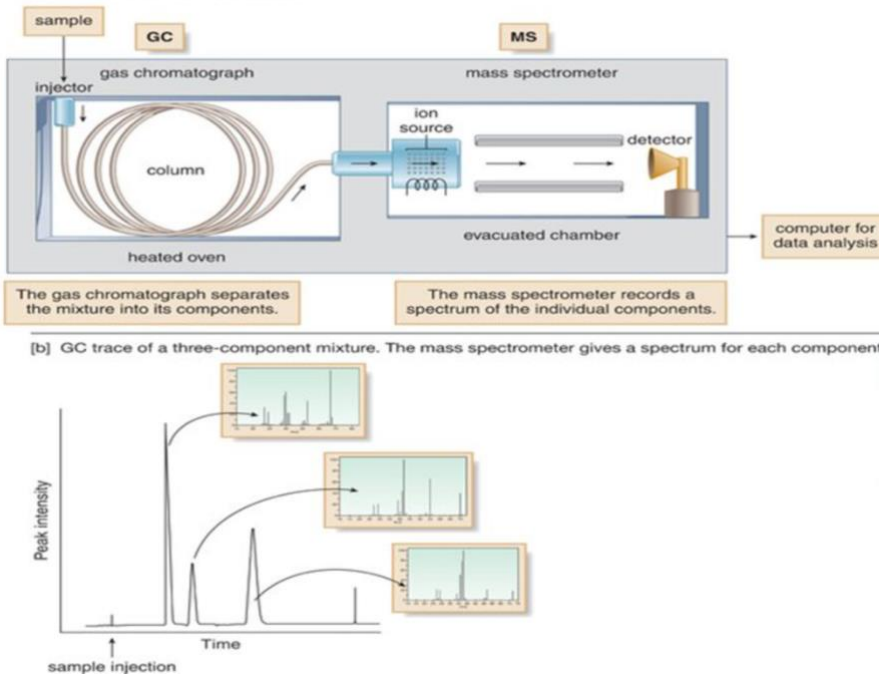

Figure 5: Schematic of a GC-MS instrumentation with mass spectra. Adopted from www.electricalwiringdiagram.com.

Preparation of fatty acid methyl esters

Methylation of free fatty acids is a common method of creating FA derivatives for GC-MS, obtained by heating FFA with a large excess of anhydrous methanol in the presence of a BF_3 catalyst [44].

1. 10-20 μL of plasma was dried under N_2 gas.
2. Under the assumption that TAGs are abundant in the plasma as we are analyzing insulin resistant models with elevated plasma TAGs, dry lipids were dissolved in 0.75 mL1:1 v/v% $CHCl_3$/MeOH and 0.25 mL BF_3/MeOH (140g of BF_3 per 1L of MeOH) (Sigma Aldrich).
3. Reaction was speeded up by heating the samples at 100°C for 5 minutes.
4. After cooling, 1 mL of ddH_2O and 2 mL of pentane (J.T. Baker) were added and samples were centrifuged at 4,000 rpm for 10 min to separate FA from other substances. FA dissolves in pentane, other impurities such as BF_3 in H_2O.
5. Pentane layer was collected by Pasteur pipette, and evaporated. 100 μL of hexane as solvent is added, solution is transferred to GC-MS insert and palmitate enrichment is analysed with GC-MS using CI.

Acetylation of hydroxyl groups

Derivatization of glycerol constituents was done by acetylation of glycerol by acetic anhydride catalyzed by pyridine in 1:1 solution.

1. 10-20 μL of plasma was combined with 100 μL of MeOH to precipitate proteins.
2. Centrifugation at max speed (17,000 rpm) and transfer of 100 μL of the volume into GC-MS vials. Solvent was evaporated as H_2O could react with acetic anhydride.
3. 75 μL of acetic anhydride/pyridine in 1:1 was added. Hydroxyl groups on glycerol are thus protected from heating in the GC-MS column by added acetate groups.
4. Heating step at 65°C for 20 min to speed up the reaction.
5. Cool down and adding of 25 μL of methanol as a solvent for GC-MS. Samples were analyzed using EI. Amount of solvent usually determines the size of the peak which corresponds to the signal strength.

Analysis

APE was measured for labelled fragment relative to unlabeled molecule and corrected for background enrichment of natural isotopes. These are essential to know since infusion of the tracer will only add to the existing background enrichment.

1. Methyl hexadecanoate: as we used +1 positive ionization for both modes, the mass of the molecular ion will equal to the molecular weight of the compound in the mass spectrum. Analysis of palmitate tracer enrichment by CI caused no significant fragmentation. Molar weight of methyl hexadecanoate is 270 g/mol, with +1 positive ionization 271 g/mol. Molar weight of [U-^{13}C]-methyl hexadecanoate was 287. Enrichment was calculated as:

$$APE = 100 \times \frac{area\ under\ the\ peak\ of\ m + 16\ (\text{labelled methyl hexadecanoate})}{area\ under\ the\ peak\ of\ m + m + 16\ (tracer + tracee)}$$

from relative areas under the eluted peaks in the mass spectrum. AUC is a value representing the abundance of the substance represented by the peak. *m* expresses tracee in the sample corrected for background isotopic isoform distribution of ^{13}C in the sample (1.11% for ^{13}C) - 272 and 273 g/mol AUCs were considered as well[43].

2. Glycerol acetate fragments

Derivatization of glycerol produces glyceryl triacetate. EI caused fragmentation at red designated spots with the molar weight of ionized the fragments 145 g/mol, 146 g/mol measured to account for 0.015% natural presence of one ^{13}C or ^{2}H isotope. 148 g/mol was the molar weight of deuterium-labelled fragment of glycerol acetate [43]. Enrichment was calculated as:

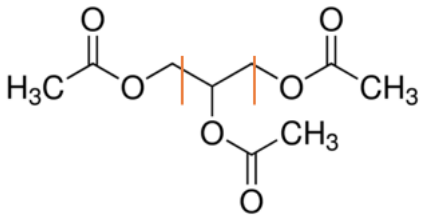

Figure 6: Glycerol fragmentation by electron ionization.

$$APE = 100 \times \frac{area\ under\ the\ peak\ of\ m + 3\ (3x\ \text{labeled glycerol triacetate})}{area\ under\ the\ peak\ of\ m + m + 3\ (tracer + tracee)}$$

GC-MS instrumentation parameters (Agilent Technologies):

Column used was HP-1 methyl siloxane 12m column (HP) with 2 μL injection into the column inlet at 250°C. Separation achieved by Helium carrier gas. Retention times for methyl hexadecanoate was 6.69 min, for glycerol triacetate 3.046 min. MS source was set into split mode 30:1 with a gas saver mode of 20 mL/min. Areas under the chromatographic peak were analyzed by mathematical integration on MSD ChemStation, Enhanced ChemStation by Agilent, with add-in LEAP EI Data Analysis with selective ion monitoring, drawing peaks of selectively desired ions.

To determine the absolute concentration of the tracer in some instances, which may be needed as the producer's purity is not always accurate, an internal standard such as [2-^{13}C]-glycerol or [1-^{14}C]-potassium palmitate is used to spike our sample at a concentration that is expected to be in the plasma. Internal standards must be labelled distinctly than tracers used.

3.1.8 Enzyme-linked immunosorbent assay of IL-6 and TNF-α

To evaluate, to what extent was lipolysis driven by inflammation, and whether the inflammation was partially suppressed by restored serum Adiponectin levels, pro-inflammatory cytokines IL-6 and TNF-α were relatively measured in plasma, subcutaneous and epididymal WAT. Mouse IL-6 and TNF-α OptEIA™ ELISA sets (BD Biosciences) with a capture anti-mouse monoclonal antibody, pre-coated to the wells and an enzyme-linked detection biotinylated anti-mouse monoclonal antibody with Streptavidin-horseradish peroxidase conjugate (SAv-HRP) were applied.

1. 100 mg of WAT was lysed in TissueLyser (Qiagen) in 500 μL of phosphate-buffered saline (PBS).
2. Samples were centrifuged at max speed (17,000 rpm) for 10 min at 4°C, 200 μ were used for ELISA, the rest for total protein concentration by Bradford assay.
3. Micro wells of a 96-well plate were coated with 100 μ of Capture Antibody diluted in coating buffer (0.1M Na_2CO_3).
4. Cells were aspirated and washed 3 times, then blocked with assay diluent (PBS with 10% fetal bovine serum (FBS)) to block non-specific binding sites on the surface.
5. 100 μL of the sample and prepared standard was applied and captured by Capture Antibody. Plate was incubated for 2 hrs at RT and then washed again 3x to remove unbound antigen.

6. 100 μL of Working Detector (Detection Antibody + SAv-HRP) was added to each well and incubated for 1 hr at RT. Detection Antibody was bound to our cytokine. Plate was then washed 7x to remove unbound antibody-enzyme conjugates.
7. 100 μL of Substrate Solution (tetramethylbenzidine and H_2O_2) was added to each well and incubated for 30 min, to react with the enzyme to form a colored complex. Reaction was stopped by 50 μL of Stop Solution (1M H_3PO_4).
8. Absorbance was read at 450 nm within 30 min with λ correction 570 nm.
The concentration was calculated with linear interpolation of the standard curve and results expressed in relative units.

3.1.9 Statistical analyses

Final data were analyzed with the help of GraphPad Prism software. Data are expressed as mean values with the standard error of the mean (SEM). Differences between the two groups were assessed using unpaired student's two tailed T-test. P-values <0.05 were considered significant.

3.2 CRMP treatment

3.2.1 Animal care, genotyping by PCR and capillary electrophoresis

All experimental procedures were approved by and conducted in accordance with the Institutional Care and Use Committee Guidelines of Yale School of Medicine. For this study, animals were handled equivalently to the conditions in section 3.1.1. Diet was HFD with an additional 7,5g/kg of CRMP, produced on demand by Research Diets Inc. as a 60% kcal% fat diet/CRMP blend, to which mice also had an *ad libitum* access.

To mimic natural conditions, housed were mutant and wild type littermates together, with a maximum of 4 mice per cage. To identify an animal's genotype and distinguish mutants from wild type mice, a specific genotyping of all study-related animals by PCR technique was performed 12 weeks prior to the study. A toe of the animal was clipped, the position of the clipping represented a unique mouse number used for later identification before sub-studies. A simplified DNA purification protocol was employed to extract DNA from the toes, as the yield was sufficient to display LMNA bands at a size of ~510 base pairs. Toes were placed into an Eppendorf tube and treated with 100μL of 50nM NaOH to digest the submerged sample for 30 min. at 95°C. Samples

were then cooled down and 10μL of Tris-HCL was introduced into the tube to neutralize the environment. After a short spin-down by centrifuge, a PCR reaction followed:

Table 1: PCR reagents and their respective amounts

Reagent	Amount (μL)
ddH_2O	18
Purified DNA	1
Fabp4-LMNA forward primer[1]	0,5
Fabp4-LMNA reverse primer[2]	0,5

1 - Nucleotide sequence (5' - 3'): ACCCCAAGGACTTTCCTTCAGA

2 - Nucleotide sequence (5' - 3'): CATTGATGAGTTTGGACAAACCAC

Reaction protocol was developed by and adapted from Mutant Mouse Resource Centre at UC Davis, California.

PCR conditions (C1000 Touch Thermal Cycler ™ by Bio-Rad):

Table 2: PCR reaction conditions

Steps	Temperature (°C)	Time (mm:ss)	Number of cycles
1. Initiation/melting	94	5:00	1
2. Denaturation	94	0:15	
3. Annealing 2-3-4 cycle in sequence	65 to 55 (↓ by 1°C per cycle)	0:30	45
4. Elongation	72	0:40	
5. Amplification	72	5:00	1
6. Finish	15	∞	n/a

The reaction was followed by an automated capillary gel electrophoresis (CE). 3,5 μL of loading dye was introduced into a directly completed PCR. CE was performed by QiAxcel Advanced Systems CE (Qiagen) which replaces a labor-intensive gel analysis with an automated system leading to a fast PCR screening, with the help of a QiAxcel DNA Fast Analysis Kit that contains prepared 2% agarose gel cartridges suited for fragments sized 15 bp - 3 kb, providing a high-resolution genotyping of up to 96

samples in 25 minutes. DNA peaks were analyzed by QiAxcel Screen Gel software. In this way, mutant mice were identified and distinguished from wild type littermates.

3.2.2 Body composition and metabolic cage study

Body composition was determined as in section 3.1.2. In addition, CRMP is a thermogenic substance which influences internal metabolic environment. It is therefore necessary to employ a Comprehensive Lab Animal Monitoring System (CLAMS, Columbus Instruments), data analyzed on Oxymax software to assess O_2 consumption, CO_2 production, animal activity and food and water intake. Gas volumes were measured by a zirconium sensor operating at 725°C, the air was recirculated for each measurement. Activity counts derived from interruption of horizontally and vertically positioned infrared laser beam, as the mouse moves within the cage. A closed el. circuit within the cage connection is distorted based on the water volume taken in by mouse. Food intake measured by a simple pressure scale. Because the measurements are bodyweight dependent, young mice are not advisable to be studied in this system, as their weight still fluctuates.

3.2.3 Intraperitoneal glucose tolerance test (IPGTT)

Glucose tolerance test is a standard established method to examine the effects of exogenous glucose delivered orally, intraperitoneally or intravenously. Following glucose administration, its systemic clearance is monitored as the levels of plasma glucose decrease with time. This directly correlates with insulin sensitivity, however, it does not determine insulin sensitivity of specific organs, as compared to clamp.

1. Animals were fasted overnight for 14 hrs.
2. 10% dextrose injection (Hospira, Inc.) diluted with saline with concentration of 1mg/g/bodyweight was injected into the intraperitoneal cavity.
3. Blood was sampled and collected by tail-bleeding each 15 mins for a total of 120 mins. The glucose clearance was then plotted, together with AUC of glucose, representing relative cumulative glucose and hence overall assessment of GTT curve [45].

3.2.4 Plasma insulin assay

Plasma from IPGTT was sent to measure the insulin concentrations in the plasma on demand, by competition insulin radioimmunoassay. The assay works on the principle of competition between radiolabeled insulin with ^{125}I and plasma insulin assayed to a given number of anti-insulin antibody binding sites adsorbed onto the walls of coated well-plate [46]. Results are expressed μU/mL.

3.2.5 Liver TAG extraction and assay

Livers were subjected to TAG extraction and assay completely in line with section 3.1.4 to assess the extent of hepatic steatosis after CRMP treatment.

3.2.6 Plasma TAG assay

10 μL of Plasma was subjected to TAG assay using 1 mL Triglyceride-SL assay reagent (Sekisui), and absorbance was read at 520nm. The concentration of TAGs was calculated from a wide standard curve using DC-Cal Multi-Analyte calibrator (Sekisui). Results were expressed in μg/μL of plasma.

3.2.7 Plasma NEFA

Plasma NEFA assay was conducted completely in line with section 3.1.3

3.2.8 Liver 2,4-DNP extraction

The efficacy of the treatment was correlated to a specific 2,4-DNP concentration in the liver, which was measured on LC-MS after 2,4-DNP was extracted. This also is considered as control measurement.

1. 100 mg of liver tissue was weighted and treated with 1,5 mL $CHCl_3$/MeOH (2:1, v/v%).
2. 40 μL of 200 μM of [3,5,6 - ^{2}H] - 2,4 DNP (Cambridge Isotopes Laboratories) as internal standard was added to each sample, which follows the 2,4-DNP through the extraction and chromatographic quantitation and acts as a calibrator on the plot of the ratio of the analyte signal to the internal standard signal. Based on known concentration of internal standard, concentration of our analyte can be precisely determined [47].

3. Livers were homogenized with TissueLyser (Qiagen). ddH_2O was added to separate DNP containing chloroform layer from the methanol layer.
4. Samples were centrifuged at 10,000 rpm, bottom organic layer containing with 2,4-DNP was and the organic solvent was evaporated with a gentle flow of N_2 gas.
5. Samples were reconstituted with 300 μL of MeOH and analyzed on LC-MS. Column used was 125mm C8 reversal HPLC column (LiChorosorb) with a 250 μL/min flow rate, 15% H_2O containing 0.1% ammonium formate and 85% MeOH. Column pressure was 1200~1300 psi.

3.2.9 Statistical analysis

Final data were analyzed with GraphPad Prism software. Data are expressed as mean values with the standard error of the mean (SEM). ANOVA with Tukey's multiple comparison test was used to determine any significant differences between the three groups. P-values <0.05 were considered significant.

4 Results

4.1 gAdiponectin treatment

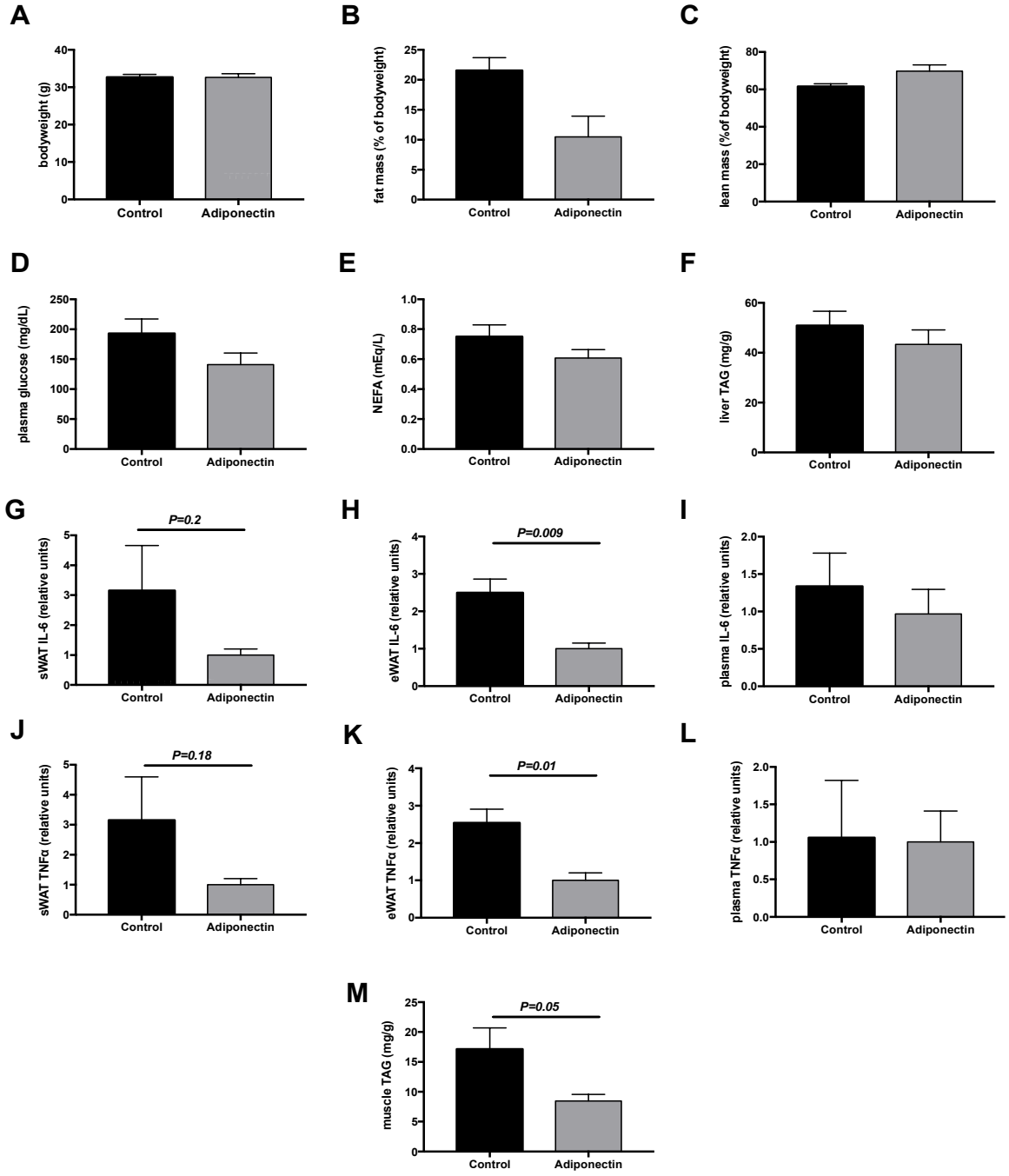

Figure 3: Basal study: subcutaneous gAdiponectin administration did not result in reversal of insulin resistance through decrease in lipolysis, regardless of the decrease in inflammation by suppression of pro-inflammatory cytokines in the basal study. A-C) Bodyweight and lean muscle mass remained unchanged, although a trend can be seen fat mass content. D) Plasma glucose levels were not normalized. E) An approximate assessment of lipolysis shows no difference in lipolysis. F and M) No reversal of hepatic steatosis, significant difference only in muscle TAGs. G-L) A clear trend can be observed, though not a significant difference in all instances, in suppression of IL-6 and TNF-α. N = 6-8 mice per group.

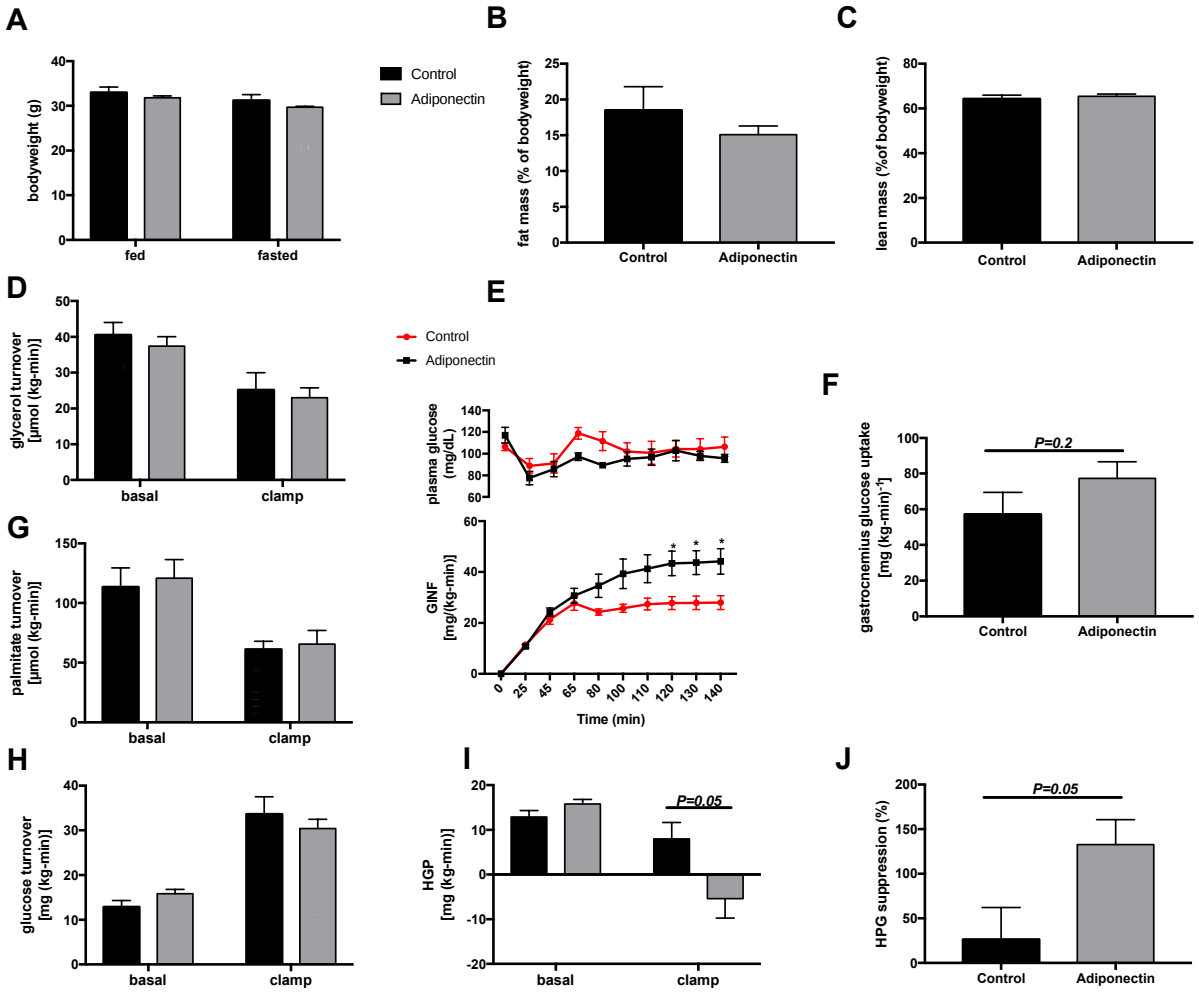

Figure 4: In-depth clamp study: gAdiponectin did not confirm the initial hypothesis, as glycerol and palmitate turnover indicates unchanged lipolysis, despite moderately suppressed inflammation and insulin-mediated HGP. A-C) The treatment did not significantly alter animal body composition. D, G) Insulin little to no effect in suppressing lipolysis as there are no changes in lipid metabolism. E-F) No significant difference in insulin-mediated plasma glucose clearance during the clamp was observed, although a slightly increased GINF in gAdiponectin treated group suggests a trend in the reversal of insulin resistance, justified by an increased muscle glucose uptake. H) Whole body glucose turnover was not different under basal nor under clamped state. I-J) It appears that adiponectin has partially restored insulin's ability to suppress HGP. N = 6-8 mice per group.

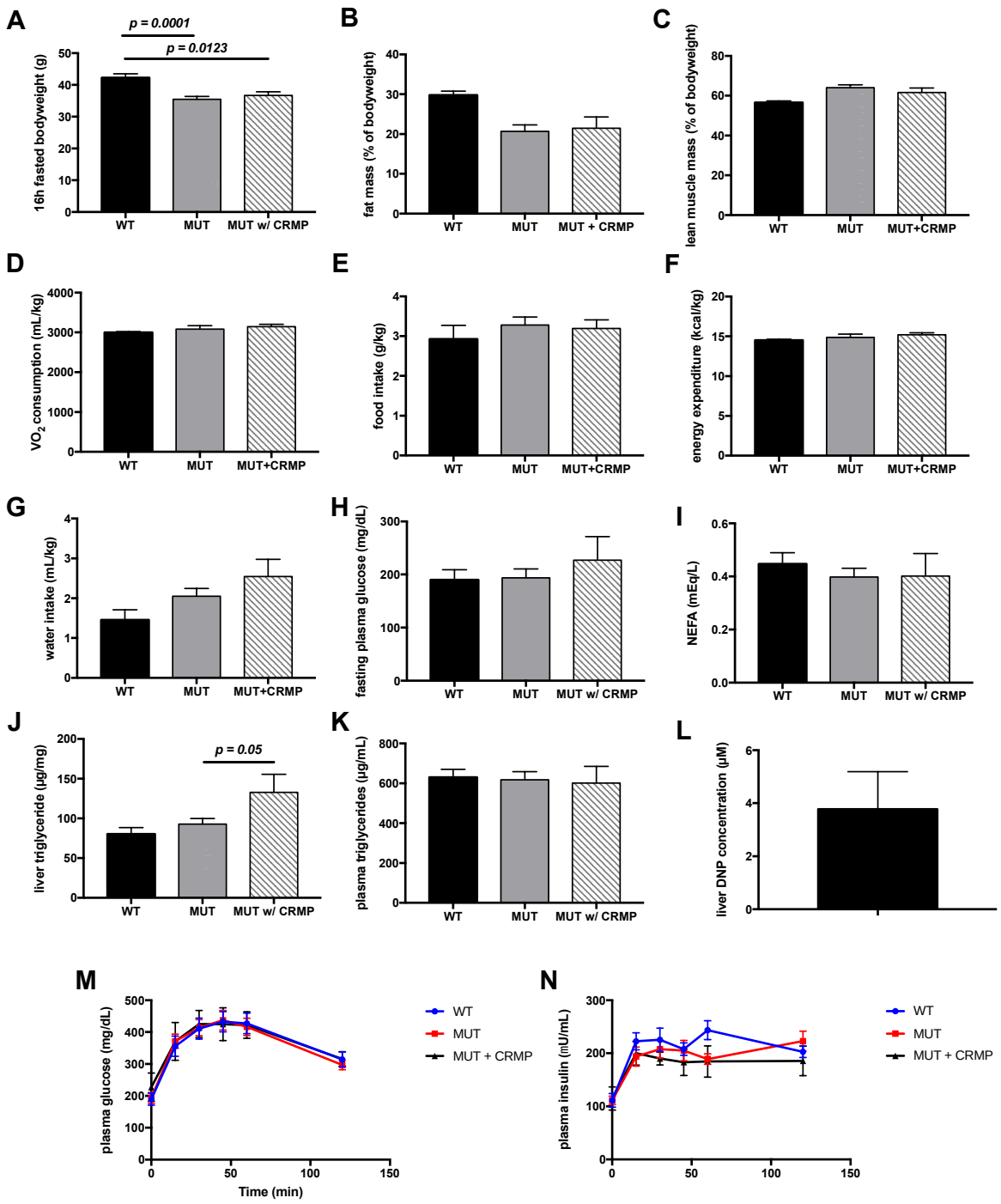

Figure 5: Oral CRMP administration did not reverse hepatic steatosis, nor did it alter insulin resistance and metabolic homeostasis, by means of thermogenesis. A) The only significant difference was observed in fasted bodyweight, which was reduced in MUT mice due to lipodystrophy. B-C) No significant difference in fat and lean muscle mass although a trend could be seen. D-G) Whole-body energy balance remained unchanged. H) HGP did not normalize as fasting glucose levels remained elevated. I) FFA remained elevated in plasma due to inflammation-mediated WAT lipolysis. J-K) No change in hepatic steatosis was observed, levels of liver and plasma triglycerides stayed high. L) Hepatic lipid extraction confirmed the presence of 2,4 DNP in the liver within the efficacious therapeutic range. M-N) Insulin resistance did not change as slow plasma glucose clearance was observed, despite high plasma insulin levels. N = 4-6 mice per group.

5 Discussion

5.1 gAdiponectin

gAdiponectin study delivered tangled results. Firstly, the treatment did not significantly alter body composition in high-fat fed animal models. Although Figure 7, B indicates a slight tendency in fat mass, it is not valid from a statistical standpoint, and the same can be seen in figure 8, B-C. Therefore, bodyweight regulatory effects cannot be ascribed to adiponectin in vivo, with our dosing.

Secondly, pro-inflammatory cytokines were clearly suppressed in gAdiponectin treated group in eWAT, with an evident tendency in sWAT, according to Figure 7, G, H, J and K, as expected [24]. The fact that this was not observed in plasma and sWAT might be explained by the mode of gAdiponectin action in plasma, as it was administered subcutaneously. However, it cannot be stated that the inflammation was suppressed from this perspective. Plasma NEFA (Figure 7, E) were elevated in both groups as well as rate of insulin-mediated plasma lipid appearance (Figure 8, D and G), indicating that insulin had little to no effect in suppressing lipolysis. This in line with the mechanism proposed by *Perry et al*. [19] (Figure 10), and conflicts with the hypothesis proposed by *Qiao et al.* [27] as adiponectin was not able to suppress PKA-HSL at this dose. TNF-α might have been effectively suppressed due to antagonistic effects of gAdipinectin [14]. One further factor causing elevated plasma NEFA in the basal study, aside from inflammation driven lipolysis, could be higher WAT TAG breakdown evoked by organism stress from Isoflurane gas anesthesia and progressive blood loss from inferior vena cava, as it is reported from experience with this in vivo method.

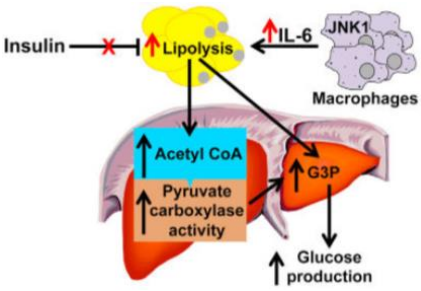

Figure 6: Macrophage accumulation impairs ability of insulin to suppress lipolysis [19].

Interestingly, there is a tendency towards a different GINF, as reflected by Figure 8, E. This implication generally is generally ascribed to insulin-stimulated muscle glucose uptake, which appears to be slightly improved in the treated group. This is also reflected by a rather higher muscle glucose uptake (Figure 8, F), although it is not statistically different. Insulin mediated whole-body glucose turnover (Figure 8, H), does not justify this phenomenon, as difference there is negligible between the groups.

However, with a significant difference in muscle TAG concentration (Figure 8, M) during the basal study, there is a sufficient evidence which points towards improved peripheral insulin resistance. Such a tendency in the treated group can be explained by increased FA oxidation in muscle tissue, as supported by *Yamauchi et al.* and *Fruebis et al.* in vitro [25, 48]. In addition, myocytes might have triggered downstream the AdipoR1 receptor mitochondrial biogenesis [26]. Improved FA oxidation could increase skeletal muscle glucose uptake by restoring myocyte insulin signaling cascade. Moreover, gAdiponectin could activate AMPK, which in turn phosphorylates ACC, which is a rate controlling step in the conversion of acetyl-CoA into malonyl-CoA. The phosphorylation of ACC inhibits ACC activity, leading to a fall in malonyl-CoA levels which disinhibit CPT-1, resulting in increased FA oxidation in the peripheral tissues [49]. Decreased live TAG concentration might correspond to a trend in decreased fat mass, as shown in Figure 7, B, despite it is not statistically meaningful. Replicating the study with increased animal numbers would most likely quantify this trend.

Lastly, it appears that there is a significant difference in HGP and consequently in insulin mediated HGP suppression (Figure 9, I-J). There are two major components regulating HGP - lipolysis and liver insulin sensitivity. Due to elevated liver TAGs in both groups (Figure 7, F), the DAG-PKCε signaling axis was not altered, meaning it must have been influenced by lipolysis. Since lipolysis stayed unchanged in both studies, difference in HGP must represent a technical experimental error, which would also explain negative HGP value, even if we account for this variance with the error bar limit. For incompletely understood reasons, measurements of glucose specific activity sometimes yield physiologically impossible negative values for HGP. To avoid this problem, some groups utilize a hot-GINF method, where [3-^{3}H]-glucose is dissolved in the glucose infusate and therefore is infused variable rate. A key limitation of this approach is to estimate the approximate steady state glucose infusion rate, and account for significantly higher costs of experiment.

5.2 CRMP treatment

Based on the efficacy of 2,4-DNP in CRMP formulation in the previous studies, the expected outcome was to observe a significantly lower hepatic TAGs in the CRMP-treated mutant group and normalized insulin resistance would have been reflected on

the GTT curve (Figure 9., M) as a sharp drop on the second time-point. However, the curve starts with fasting plasma glucose levels at ~200 mg/dL, which almost double of what an insulin sensitive mouse would exhibit (90 - 100 mg/dL). Consistent with this finding, plasma insulin levels remained elevated in all groups. In opposition to our expectation, liver TAGs (Figure 9., J) were even higher in the treated group, regardless of hepatic DNP concentration within the efficacious range. The only significant difference was seen in the fasted bodyweight, which might be explained by lack of fat accumulation due to defect in adipocyte maturation in combination with the DNP-induced thermogenesis. This might also correlate with a trend in decreased fat mass, as seen in Figure 9., B. The whole-body energy balance remained unchanged.

Altogether, the treatment was insufficient to reverse insulin resistance, nor to alter any of the given insulin resistance indicators. We currently hypothesize, that the treatment length might have been inappropriate, or, that the extent of NAFLD caused by that long high-fat feeding (8 weeks) was too severe to be countered with the given drug dosage. Therefore, shortening the length of high-fat feeding or increasing the DNP dosage could be a viable way to further assess these findings and draw a pertinent conclusion. Since a rather acute CRMP treatment has been shown to work effectively to reverse diabetes [32], the length of 6 weeks might have caused a mitochondrial adaptation to the mechanism of this treatment in the long-term, in a yet unknown way. Interesting option would also be to simultaneously analyze and compare the brown adipose tissue (BAT), which has a thermogenic function, improves glucose homeostasis and insulin sensitivity, and might also have been influenced by the CRMP treatment.

6 Conclusion

These results provide proof-of-concept data for this approach for the reversal of insulin resistance. In vivo effects gAdiponectin on hepatic and peripheral metabolism were investigated for the first time, and due to the resulting tendencies, the study now is in a secondary stage. Effects on muscle tissue mitochondrial oxidation after 2-week treatment with equal gAdiponectin dose is currently being examined by repeated 2-deoxy-D-[1-^{14}C]-glucose bolus infusion and novel TCA cycle flux analysis of mitochondrial citrate synthase flux and pyruvate carboxylase flux by positional isotopomer NMR tracer analysis [50]. This is being done on 32 mice for a basal and a clamp study.

TNF-α and IL-6 are being evaluated together with PKCθ translocation in the muscle as well as tissue DAGs and TAGs to assess hepatic steatosis and insulin signaling cascade in detail.

With regards to the future of CRMP as a liver-targeted uncoupling agent, the problem a long-term administration of this drug needs to be addressed after this study, and, in a case of inefficiency, therapy optimized with a methyl-ester modulation of DNP (DNP-ME), which was initially the viable option [20]. Alternatively, ACC inhibitors are being investigated by this laboratory as an effective target of hepatic lipogenesis which facilitate the import of FA and thereby regulate lipid oxidation and hepatic DNL [51]
Despite this plethora of therapeutic options, the most clinically established ones which address the root cause of insulin resistance is weight loss by diet with caloric restriction, aerobic exercise or bariatric surgery, all of which ameliorate ectopic lipid accumulation in the span of several months [20].

In conclusion, insulin resistance is a complex condition which is also underlined by an evolutionary basis, as a starved organism strives to preserve carbohydrates for the brain and triggers peripheral and hepatic insulin resistance by the outlined mechanism. It might therefore take longer to fully implement an efficient pharmacologic strategy to modulate such a series of physiological events, in order to successfully improve life quality of patients suffering from NAFLD, diabetes and other related conditions.

References

1. James, W.P.T., *WHO recognition of the global obesity epidemic.* International Journal Of Obesity, 2009. **32**: p. S120.
2. Wong, R.J., C. Chou, and A. Ahmed, *Long term trends and racial/ethnic disparities in the prevalence of obesity.* J Community Health, 2014. **39**(6): p. 1150-60.
3. Wu, Y., et al., *Risk factors contributing to type 2 diabetes and recent advances in the treatment and prevention.* Int J Med Sci, 2014. **11**(11): p. 1185-200.
4. Samuel, V.T. and G.I. Shulman, *The pathogenesis of insulin resistance: integrating signaling pathways and substrate flux.* J Clin Invest, 2016. **126**(1): p. 12-22.
5. Tolman, K.G., et al., *Spectrum of liver disease in type 2 diabetes and management of patients with diabetes and liver disease.* Diabetes Care, 2007. **30**(3): p. 734-43.
6. Petersen, K.F., et al., *Increased prevalence of insulin resistance and nonalcoholic fatty liver disease in Asian-Indian men.* Proc Natl Acad Sci U S A, 2006. **103**(48): p. 18273-7.
7. Das, K., et al., *Nonobese population in a developing country has a high prevalence of nonalcoholic fatty liver and significant liver disease.* Hepatology, 2010. **51**(5): p. 1593-1602.
8. Bloomgarden, Z.T., *Nonalcoholic fatty liver disease and insulin resistance in youth.* Diabetes Care, 2007. **30**(6): p. 1663-9.
9. Shulman, G.I., *Ectopic fat in insulin resistance, dyslipidemia, and cardiometabolic disease.* N Engl J Med, 2014. **371**(23): p. 2237-8.
10. Garg, A., *Clinical review#: Lipodystrophies: genetic and acquired body fat disorders.* J Clin Endocrinol Metab, 2011. **96**(11): p. 3313-25.
11. Wojtanik, K.M., et al., *The role of LMNA in adipose: a novel mouse model of lipodystrophy based on the Dunnigan-type familial partial lipodystrophy mutation.* J Lipid Res, 2009. **50**(6): p. 1068-79.
12. Weltman, M.D., et al., *Hepatic cytochrome P450 2E1 is increased in patients with nonalcoholic steatohepatitis.* Hepatology, 1998. **27**(1): p. 128-33.
13. Bataller, R. and D.A. Brenner, *Liver fibrosis.* J Clin Invest, 2005. **115**(2): p. 209-18.
14. Hui, J.M., et al., *Beyond insulin resistance in NASH: TNF-alpha or adiponectin?* Hepatology, 2004. **40**(1): p. 46-54.
15. El-Serag, H.B. and J.E. Everhart, *Diabetes increases the risk of acute hepatic failure.* Gastroenterology, 2002. **122**(7): p. 1822-8.
16. Browning, J.D., et al., *Prevalence of hepatic steatosis in an urban population in the United States: impact of ethnicity.* Hepatology, 2004. **40**(6): p. 1387-95.
17. Oseini, A.M. and A.J. Sanyal, *Therapies in non-alcoholic steatohepatitis (NASH).* Liver International, 2017. **37**: p. 97-103.
18. Perry, R.J., et al., *The role of hepatic lipids in hepatic insulin resistance and type 2 diabetes.* Nature, 2014. **510**(7503): p. 84-91.
19. Perry, R.J., et al., *Hepatic acetyl CoA links adipose tissue inflammation to hepatic insulin resistance and type 2 diabetes.* Cell, 2015. **160**(4): p. 745-58.
20. Samuel, V.T. and G.I. Shulman, *Nonalcoholic Fatty Liver Disease as a Nexus of Metabolic and Hepatic Diseases.* Cell Metab, 2018. **27**(1): p. 22-41.
21. Samuel, V.T., et al., *Mechanism of hepatic insulin resistance in non-alcoholic fatty liver disease.* J Biol Chem, 2004. **279**(31): p. 32345-53.

22. Kraegen, E.W., et al., *Development of muscle insulin resistance after liver insulin resistance in high-fat-fed rats.* Diabetes, 1991. **40**(11): p. 1397-403.
23. Lihn, A.S., S.B. Pedersen, and B. Richelsen, *Adiponectin: action, regulation and association to insulin sensitivity.* Obes Rev, 2005. **6**(1): p. 13-21.
24. Maeda, N., et al., *Diet-induced insulin resistance in mice lacking adiponectin/ACRP30.* Nat Med, 2002. **8**(7): p. 731-7.
25. Fruebis, J., et al., *Proteolytic cleavage product of 30-kDa adipocyte complement-related protein increases fatty acid oxidation in muscle and causes weight loss in mice.* Proc Natl Acad Sci U S A, 2001. **98**(4): p. 2005-10.
26. Iwabu, M., et al., *Adiponectin and AdipoR1 regulate PGC-1alpha and mitochondria by Ca(2+) and AMPK/SIRT1.* Nature, 2010. **464**(7293): p. 1313-9.
27. Qiao, L., et al., *Adiponectin inhibits lipolysis in mouse adipocytes.* Diabetes, 2011. **60**(5): p. 1519-27.
28. Holland, W.L., et al., *Receptor-mediated activation of ceramidase activity initiates the pleiotropic actions of adiponectin.* Nat Med, 2011. **17**(1): p. 55-63.
29. Berg, A.H., et al., *The adipocyte-secreted protein Acrp30 enhances hepatic insulin action.* Nat Med, 2001. **7**(8): p. 947-53.
30. Xu, A., et al., *The fat-derived hormone adiponectin alleviates alcoholic and nonalcoholic fatty liver diseases in mice.* J Clin Invest, 2003. **112**(1): p. 91-100.
31. Grundlingh, J., et al., *2,4-dinitrophenol (DNP): a weight loss agent with significant acute toxicity and risk of death.* J Med Toxicol, 2011. **7**(3): p. 205-12.
32. Perry, R.J., et al., *Controlled-release mitochondrial protonophore reverses diabetes and steatohepatitis in rats.* Science, 2015. **347**(6227): p. 1253-6.
33. Abulizi, A., et al., *A controlled-release mitochondrial protonophore reverses hypertriglyceridemia, nonalcoholic steatohepatitis, and diabetes in lipodystrophic mice.* FASEB J, 2017. **31**(7): p. 2916-2924.
34. Boden, G., *Free fatty acids (FFA), a link between obesity and insulin resistance.* Front Biosci, 1998. **3**: p. d169-75.
35. Kim, J.K., *Hyperinsulinemic–Euglycemic Clamp to Assess Insulin Sensitivity In Vivo*, in *Type 2 Diabetes: Methods and Protocols*, C. Stocker, Editor. 2009, Humana Press: Totowa, NJ. p. 221-238.
36. Ayala, J.E., et al., *Hyperinsulinemic-euglycemic clamps in conscious, unrestrained mice.* J Vis Exp, 2011(57).
37. Vella, A. and R.A. Rizza, *Application of Isotopic Techniques Using Constant Specific Activity or Enrichment to the Study of Carbohydrate Metabolism.* Diabetes, 2009. **58**(10): p. 2168-2174.
38. Khan, A.H. and J.E. Pessin, *Insulin regulation of glucose uptake: a complex interplay of intracellular signalling pathways.* Diabetologia, 2002. **45**(11): p. 1475-83.
39. *Beckman Instruments 5801 Series Liquid Scintillation Systems Operating Manual*. LS 1801. 1985.
40. Chapon, A., et al., *Optimization of liquid scintillation measurements applied to smears and aqueous samples collected in industrial environments.* Results in Physics, 2016. **6**: p. 50-58.
41. Koutsari, C. and M.D. Jensen, *Thematic review series: patient-oriented research. Free fatty acid metabolism in human obesity.* J Lipid Res, 2006. **47**(8): p. 1643-50.
42. Umpleby, A.M., *HORMONE MEASUREMENT GUIDELINES: Tracing lipid metabolism: the value of stable isotopes.* J Endocrinol, 2015. **226**(3): p. G1-10.

43. Schierbeek, H., *Mass Spectrometry and Stable Isotopes in Nutritional and Pediatric Research*, H. Schierbeek, Editor. 2017, Wiley: Hoboken, New Jersey. p. 376.
44. Morrison, W.R. and L.M. Smith, *Preparation of Fatty Acid Methyl Esters and Dimethylacetals from Lipids with Boron Fluoride--Methanol.* J Lipid Res, 1964. **5**: p. 600-8.
45. Andrikopoulos, S., et al., *Evaluating the glucose tolerance test in mice.* Am J Physiol Endocrinol Metab, 2008. **295**(6): p. E1323-32.
46. Kagan, A., *Radioimmunoassay of insulin.* Semin Nucl Med, 1975. **5**(2): p. 183-8.
47. Wieling, J., *LC-MS-MS experiences with internal standards.* Journal of Chromatographia, 2002. **55(suppl 1)**: p. pp S107-S113.
48. Yamauchi, T., et al., *The fat-derived hormone adiponectin reverses insulin resistance associated with both lipoatrophy and obesity.* Nat Med, 2001. **7**(8): p. 941-6.
49. Kahn, B.B., et al., *AMP-activated protein kinase: ancient energy gauge provides clues to modern understanding of metabolism.* Cell Metab, 2005. **1**(1): p. 15-25.
50. Perry, R.J., et al., *Non-invasive assessment of hepatic mitochondrial metabolism by positional isotopomer NMR tracer analysis (PINTA).* Nat Commun, 2017. **8**(1): p. 798.
51. Savage, D.B., et al., *Reversal of diet-induced hepatic steatosis and hepatic insulin resistance by antisense oligonucleotide inhibitors of acetyl-CoA carboxylases 1 and 2.* J Clin Invest, 2006. **116**(3): p. 817-24.